UNIVERSITY OF LEEDS

This is a repository copy of *Mechanically Tuneable Physical Nanocomposite Hydrogels from Polyelectrolyte Complex Templated Silica Nanoparticles for Anionic Therapeutic Delivery*.

White Rose Research Online URL for this paper:
https://eprints.whiterose.ac.uk/184022/

Version: Accepted Version

Article:
Newham, G orcid.org/0000-0002-4877-5513, Evans, SD orcid.org/0000-0001-8342-5335 and Ong, ZY orcid.org/0000-0001-8666-4382 (2022) Mechanically Tuneable Physical Nanocomposite Hydrogels from Polyelectrolyte Complex Templated Silica Nanoparticles for Anionic Therapeutic Delivery. Journal of Colloid and Interface Science, 617. pp. 224-235. ISSN 0021-9797

https://doi.org/10.1016/j.jcis.2022.02.052

© 2022, Elsevier. This manuscript version is made available under the CC-BY-NC-ND 4.0 license http://creativecommons.org/licenses/by-nc-nd/4.0/.

Reuse
This article is distributed under the terms of the Creative Commons Attribution-NonCommercial-NoDerivs (CC BY-NC-ND) licence. This licence only allows you to download this work and share it with others as long as you credit the authors, but you can't change the article in any way or use it commercially. More information and the full terms of the licence here: https://creativecommons.org/licenses/

Takedown
If you consider content in White Rose Research Online to be in breach of UK law, please notify us by emailing eprints@whiterose.ac.uk including the URL of the record and the reason for the withdrawal request.

White Rose university consortium
Universities of Leeds, Sheffield & York

eprints@whiterose.ac.uk
https://eprints.whiterose.ac.uk/

Mechanically Tuneable Physical Nanocomposite Hydrogels from Polyelectrolyte Complex Templated Silica Nanoparticles for Anionic Therapeutic Delivery

George Newham[1], Stephen D. Evans[1], Zhan Yuin Ong*[1,2]

1 School of Physics and Astronomy, University of Leeds, Leeds, LS2 9JT, UK.

2 Leeds Institute of Medical Research at St. James's, School of Medicine, University of Leeds, Leeds, LS2 9JT, UK.

*Correspondence to: Z.Y. Ong (z.y.ong@leeds.ac.uk)

Abstract

Hydrogels have shown great promise for drug delivery and tissue engineering but can be limited in practical applications by poor mechanical performance. The incorporation of polymer grafted silica nanoparticles as chemical or physical crosslinkers in *in situ* polymerised nanocomposite hydrogels has been widely researched to enhance their mechanical properties. Despite the enhanced mechanical stiffness, tensile strength, and self-healing properties, there remains a need for the development of simpler and modular approaches to obtain nanocomposite hydrogels. Herein, we report a facile protocol for the polyelectrolyte complex (PEC) templated synthesis of organic-inorganic hybrid poly(ethylenimine) functionalised silica nanoparticles (PEI-SiNPs) and their use as multifunctional electrostatic crosslinkers with hyaluronic acid (HA) to form nanocomposite hydrogels. Upon mixing, electrostatic interactions between cationic PEI-SiNPs and anionic HA resulted in the formation of a coacervate nanocomposite hydrogel with enhanced mechanical stiffness that can be tuned by varying the ratios of PEI-SiNPs and HA present. The reversible electrostatic interactions within the hydrogel networks also enabled self-healing and thixotropic properties. The excess positive charge present within the PEI-SiNPs facilitated high loading and retarded the release of the anionic anti-cancer drug methotrexate from the nanocomposite hydrogel. Furthermore, the electrostatic complexation of PEI-SiNP and HA was found to mitigate haemotoxicity concerns associated with the use of high molecular weight PEI. The method presented herein

offers a simpler and more versatile strategy for the fabrication of coacervate nanocomposite hydrogels with tuneable mechanical stiffness and self-healing properties for drug delivery applications.

1. Introduction

Hydrogels are three-dimensional water swollen networks formed from the chemical or physical crosslinking of hydrophilic polymers. Their high water content, porosity, tuneable physiochemical properties, and capacity to encapsulate drugs and cells make them valuable for a wide range of biological applications such as tissue engineering[1], bioadhesive gels and wound healing[2], and therapeutic delivery[3]. However, the successful translation of many hydrogel systems has been limited by poor mechanical properties such as insufficient stiffness, brittleness, and lack of self-healing properties due to the heterogeneous distribution of crosslinking points and the inability of the hydrogel networks to dissipate energy.[4,5]

To improve the mechanical properties and confer added functionalities, nanocomposite hydrogels incorporating silica nanoparticles (SiNPs)[6–8], polymeric nanoparticles[9], gold nanoparticles[10], iron oxide nanoparticles[11], and carbon nanotubes[12] have been utilised. Amongst the various nanoparticle types, SiNPs are most promising for improving the mechanical performance of nanocomposite hydrogels in biomedical applications due to their inherent biocompatibility, biodegradability, colloidal stability, and ease of synthesis. The most common methods of preparing mechanically robust nanocomposite hydrogels include chemical and/or physical crosslinking of SiNPs with polymeric gelators. In chemically crosslinked nanocomposite hydrogels, surface modified SiNPs are typically used for the covalent grafting of polymers via free radical polymerisation or for crosslinking with polymers bearing complementary functional groups through photo-crosslinking of methacrylates, thiol-thiol, and aldehyde-amine bonds.[8,13–17] Yang *et al.* reported tough and elastic nanocomposite hydrogels formed by the *in situ* covalent grafting of poly(acrylic acid) (PAA) from vinyl functionalised SiNPs.[8] The polymer-bridged SiNPs acted as multifunctional crosslinking points, enabling the dynamic disentanglement of the PAA chains to facilitate energy dissipation during deformation. Although tough and flexible hydrogels were obtained, predominantly chemically crosslinked hydrogels formed via permanent covalent bonds tend to lack

self-healing and thixotropic properties that are desirable for *in vivo* biomedical applications.

In physical nanocomposite hydrogels, SiNPs are incorporated into the network via electrostatic interactions, hydrophobic interactions, hydrogel bonding, and/or Van der Waal's forces.[6,18–20] Although SiNPs may be simply embedded into physical hydrogel formulations without any engineered intermolecular interactions or crosslinking, such systems have yielded weak mechanical reinforcement.[21,22] In contrast, the design of polymer grafted SiNPs as physical crosslinkers for interaction with polymer chains confers desirable mechanical attributes. Zheng *et al.* reported the use of poly(2-dimethylaminoethyl methacrylate) modified SiNPs (SiO_2@PDMAEMA) as multifunctional crosslinkers in an *in situ* polymerised PAA network.[6] The electrostatic interactions between the SiO_2@PDMAEMA and PAA resulted in a supramolecular nanocomposite hydrogel with high tensile strength and self-healing properties. Ternary crosslinked nanocomposite hydrogels formed from the *in situ* copolymerisation of acrylamide and stearyl methacrylate monomers on vinyl functionalised SiNPs have also been reported.[20] In this system, the hydrogel network is formed by hydrogen bonding and hydrophobic interactions between the grafted co-polymer chains and covalent bonds between the SiNPs. Despite the improved mechanical properties observed for the aforementioned SiNP crosslinked nanocomposite hydrogels, the requirement for toxic monomers, initiators and catalysts and/or high temperatures for the *in situ* polymerisation process may limit biological applications and the loading of thermally labile drugs.[8,20] In addition, the sequestration of free radicals by the SiNPs during the free radical polymerisation could also affect reproducibility of the hydrogel synthesis and mechanical properties.[23] The current synthesis of the polymer brush grafted SiNP crosslinkers also requires multiple steps involving the Stöber synthesis of the SiNPs, followed by surface modification which could increase the time and cost of production.[6,8] There is thus a need for a simpler and modular approach to produce nanocomposite hydrogels with tuneable mechanical stiffness and self-healing properties for biomedical applications.

In this study, we present a novel protocol for the formation of mechanically tuneable and self-healing nanocomposite hydrogels using organic-inorganic hybrid

poly(ethylenimine) functionalised SiNPs (PEI-SiNPs) as multifunctional crosslinkers for electrostatic interaction with hyaluronic acid (HA). We have recently reported the synthesis of monodispersed SiNPs using PAA/arginine polyelectrolyte complexes (PECs) as templates for silane mineralisation.[24] Here, PECs formed from PEI and glutamic acid (Glu) were used as scaffolds for the one-pot synthesis of uniform core-shell PEI-SiNPs (Scheme 1). Electrostatic interactions between cationic PEI and anionic HA led to the formation of a polymer-rich coacervate phase and its subsequent syneresis, yielding an electrostatically crosslinked physical hydrogel with reinforced and tuneable mechanical stiffness. Importantly, the reversible ionic bonds between the PEI-SiNP and HA in the nanocomposite hydrogel afforded the dynamic network properties required for shear thinning and self-healing. In addition to its role in gelation, the surplus of charged amines present in the PEI-SiNPs enhanced the loading and subsequent release of the anionic anticancer drug methotrexate (MTX) following hydrogel formation.

The incorporation of PEI-SiNPs into the coacervate hydrogel network and its influence on the conditions required for gelation were systematically investigated. The equilibrium swelling and rheological properties of the nanocomposite hydrogels formed from different PEI-SiNP:HA concentration ratios were studied in comparison to PEI/HA hydrogels (not associated with SiNPs) and HA. Subsequently, the haemocompatibility as well as drug loading and release profiles of the nanocomposite hydrogels were evaluated. This work provides important insight into the design and preparation of physically crosslinked nanocomposite hydrogel drug delivery systems and the interplay between their physical and application specific properties.

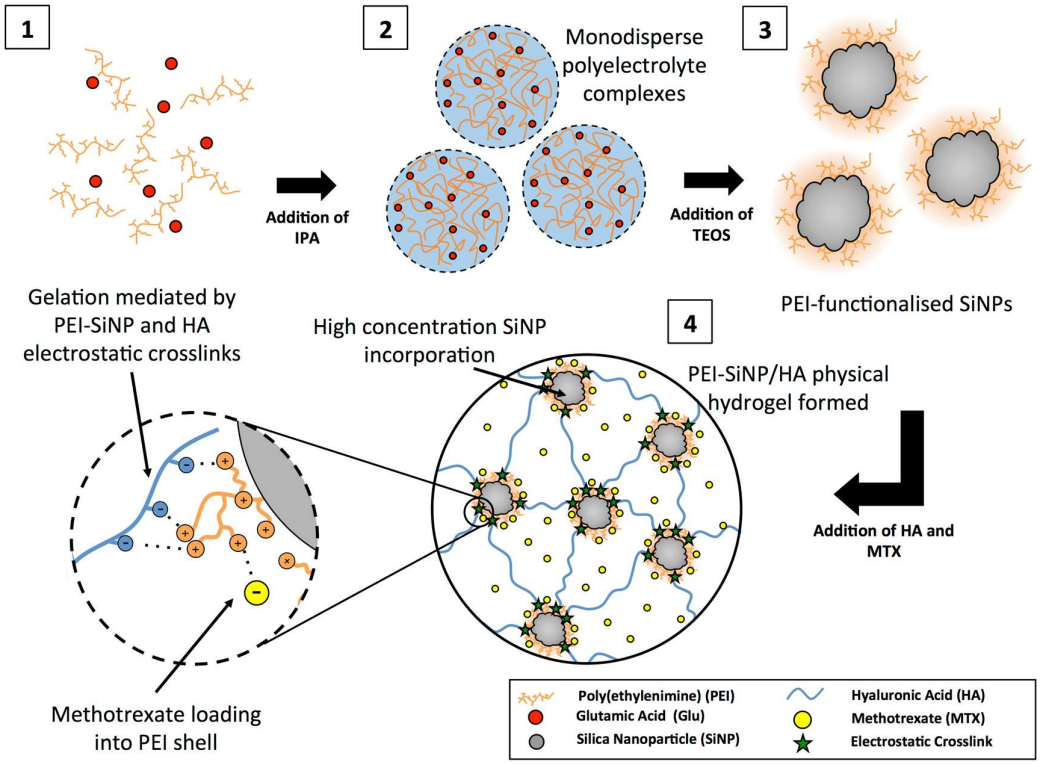

Scheme 1 A graphical representation of the PEC templated synthesis of core-shell PEI-SiNPs and their subsequent use as multifunctional crosslinking junctions in the formation of coacervate nanocomposite hydrogels. (1) PEI and Glu are initially mixed in an aqueous solution before (2) the addition of isopropanol (IPA) to form monodispersed nanoscale PECs. (3) On the addition of TEOS, the silanes selectively condense inside the PECs and each one becomes a PEI-functionalised SiNP (PEI-SiNP). (4) The PEI-SiNPs are mixed with HA and MTX to form a drug loaded, physical nanocomposite hydrogel with electrostatic crosslinks.

2. Materials and Methods

2.1 Materials

Branched polyethylenimine (PEI; M_w = 25,000, M_n = 10,000), Sodium hydroxide (pellets; ≥ 98 %), cetrimonium bromide (CTAB; ≥ 98%), and polyacrylic acid (PAA; M_w = 1800) were purchased from Sigma Aldrich. Glutamic acid (Glu; 99%), L-Arginine (Arg; 98%), and phosphoric acid (85%) were purchased from Acros Organics. 2-propanol (IPA; 99.7%) was purchased from VWR. Tetraethoxysilane (TEOS; 99.9%) and hyaluronic acid sodium salt (HA; streptococcus equi, 91%, $M_w \geq 1.0 \times 10^6$ Da) were purchased form Alfa Aesar. Methotrexate sodium salt (MTX) was purchased from Toku-E, and Coomassie brilliant blue g-250 (CBBG) was purchased

form Cayman Chemical Company. Ultrapure water (Millipore Milli-Q) with 18.2 M Ω·cm resistivity at 25 °C was used in all experiments.

2.2 Synthesis of PEI-SiNPs

For the synthesis of PEI-SiNPs, PEC templates were prepared with 12.5 mL of 1.28×10^0 mM PEI and 5 mL of 5.45×10^1 mM Glu in a 250 mL total volume of 80% IPA (v/v). With the temperature maintained at 40 °C in a water bath, 1 mL of TEOS was added under stirring. After 24 h, the final product was purified by centrifugation at 17,000 × g for 1 h and rinsed thrice with ultrapure water.

2.3 Characterisation of PECs and PEI-SiNPs

The hydrodynamic diameters, polydispersity indices, and zeta potentials of the PECs and PEI-SiNPs were determined with dynamic light scattering (DLS) using the Zetasizer Nano with scattered light from a He-Ne laser detected at 173° (Malvern Instrument Ltd., Worcestershire, UK). The results are presented as the mean ± standard deviation of three runs each of at least 12 measurements at 25 °C. SiNP morphology and size analysis was completed with high resolution TEM (FE Tecnai G2-Spirit) operating at 120 KeV with a tungsten filament and a Gatan Ultrascan 4000 CCD camera. Typically, 5 μL of as-synthesised sample was pipetted onto a carbon coated copper grid and dried under nitrogen flow at room temperature before imaging. The particle size distribution was assessed from the TEM images using ImageJ analysis software. The smallest possible ellipse was drawn around each particle and the major axis length was quoted as the particle size. The FTIR spectra were collected using the Thermo Scientific Nicolet iS10 between 650 – 4000 cm^{-1} with a spectral resolution of 2 cm^{-1}. The particles were lyophilised and combined with KBr to form a pellet used for analysis. The organic functionalities within the SiNPs were analysed with thermogravimetric analysis (TGA) using the Mettler Toledo TGA/DSC1 Star System. For measurement, lyophilised particles of known mass were added to a crucible of known mass and heated between 30 – 700 °C at a heating rate of 10 °C min^{-1} under nitrogen flow. Reported spectra are shown between 150 – 700 °C to omit contributions from residual water adsorbed during sample preparation. For Cryo-SEM analysis, hydrogel samples were frozen in a liquid nitrogen slush, fractured, and

sublimated at -50 °C for 2 minutes with the Quorum PP3010 before sputter coating with iridium (5 mA for 60 s). Imaging was performed with the FEI Helios G4 CX.

2.4 PEI-SiNP/HA Hydrogel Formation

For the preparation of PEI-SiNP/HA gels with a PEI:HA monomer ratio of 2.4:4.8, 200 µL of PEI-SiNP stock containing 67.2 µM of silica surface bound PEI (3.65 mM PEI monomers) and 58.4 µL of 10 µM HA (25 mM HA monomers) were added to 36.6 µL of ultrapure water. After mixing using a vortex mixer, a suspension of white precipitates was formed. To this, 5 µL of 2 M hydrochloric acid was added (total volume 300 µL) to tune the pH to ~ 6 before further mixing with a vortex mixer to induce the formation of a coacervate hydrogel. Syneresis occurred to result in a white hydrogel suspended in a colourless supernatant. For the synthesis of PEI/HA gels, the same protocol was followed but with an equimolar solution of PEI in place of PEI-SiNPs. For the formation of gels with varied PEI and HA concentration the total volume was maintained at 300 µL.

The cation:anion charge ratio for the as-synthesised hydrogels was calculated from the protonation state of each functional group at pH 6 determined from the Henderson-Hasselbalch equation:

$$pH = pK_a + \log([base]/[acid]) \quad (1)$$

2.5 Quantification of SiNP surface-bound PEI concentration

To prepare a stock of Coomassie stain, 8.5 mg of CBBG was dissolved in 4.1 mL of 95% ethanol and added to 8.4 mL of 85% phosphoric acid and 37.5 mL of ultrapure water. To quantify the concentration of PEI conjugated to the PEI-SiNP surface, 200 µL of Coomassie stock solution was added to 100 µL of diluted SiNP dispersion in a 96 well plate and after 5 min incubation, the absorbance was measured at 595 nm. The concentration of PEI at the PEI-SiNP surface was determined by comparison of absorbance values to a calibration curve of known PEI concentrations.

2.6 Quantification of PEI Remaining in Supernatant after Hydrogel Formation with Coomassie Assay

To quantify the residual PEI after hydrogel formation, 200 µL of Coomassie stain (prepared as described in section 2.5) was added to 100 µL of diluted supernatant collected after hydrogel formation, in a 96 well plate. After incubation for 5 min, the optical absorbance was measured at 595 nm and compared to a calibration curve of known PEI concentrations.

2.7 Quantification of HA Remaining in Supernatant after Hydrogel Formation with CTAB Turbidity Assay

To evaluate the concentration of HA in the gel supernatants, the CTAB turbidimetric method was used[25]. The assay solution was prepared by dissolving 2.5 g of CTAB in 100 mL of 2% (w/v) NaOH. 100 µL of CTAB solution was added to 50 µL of the hydrogel supernatant in a 96 well plate and incubated for 10 min. The absorbance was measured at 600 nm and compared to a calibration curve of known HA concentrations.

2.8 Hydrogel Swelling Ratio

Freshly prepared hydrogel samples in the swollen state were weighed before drying under nitrogen flow and then in an oven at 50 °C overnight. Hydrogels were considered dry when the weighed mass stopped decreasing. The dried gels were then weighed and the swelling ratio was calculated from three replicates using the equation as follows:

$$\text{Swelling Ratio (\%)} = [(\text{Swollen Mass})/(\text{Dried Mass})] \times 100 \quad (2)$$

2.9 Haemolysis Testing

Whole blood obtained from mice was diluted 25 × with 1 × PBS to obtain a 4% v/v suspension. 0.5 mL of the diluted blood suspension was added to each hydrogel. The samples were incubated for 1 h at 37 °C before centrifugation at 1000 × g for 5 min. 0.1 mL of the supernatant was subsequently transferred to each well of a 96-well plate. The absorbance was measured at 576 nm using a microplate spectrophotometer (Molecular Devices SpectraMax M2e). Whole blood suspension incubated with PBS was used as negative control and red blood cells lysed with 0.05 % v/v Triton X-100 was used as the positive control. The percentage haemolysis was calculated using the following formula:

Haemolysis (%) = [(OD576 nm of hydrogel sample − OD576 nm of negative control)/(OD576 nm of positive control − OD576 nm of negative control)] × 100 (3)

2.10 Rheology

The rheological properties of PEI/HA and PEI-SiNP/HA hydrogels were characterised with the Anton Paar MCR 302. Freshly prepared hydrogels were used with an 8 mm parallel plate geometry and a 0.5 mm gap at 20 °C for all experiments. Frequency sweep measurements were performed at 1 % shear strain between 0.1 – 10 Hz, and strain sweep measurements were performed at a frequency of 1 Hz between 1 – 1000% shear strain. The self-healing properties of the hydrogels were assessed with cyclical low (1%) and high (1000%) shear strain periods of 30 s at a frequency of 1 Hz.

2.11 Macroscopic Self-Healing Test

To demonstrate the macroscopic self-healing of PEI-SiNP/HA nanocomposite hydrogels, two hydrogels were prepared with and without CBBG dye. For the incorporation of blue dye into the hydrogel, 30 µL of 0.1 mg mL^{-1} CBBG was added to the PEI-SiNPs prior to the addition of HA and HCl described in section 2.4. The freshly prepared hydrogels were cut with a scalpel and the cut surfaces were placed together in close contact in a sealed container at room temperature. After 1 h, the hydrogel was suspended under its own weight and stretched by hand to test the network healing.

2.12 Drug Loading and Release

The anticancer drug MTX was incorporated during hydrogel formation. 10 µL of 33 mg mL^{-1} MTX aqueous solution and 200 µL of PEI-SiNP stock containing 67.2 µM of silica surface bound PEI were combined and then added to 58.4 µL of 10 µM HA and 26.6 µL of ultrapure water before mixing with a vortex mixer. 5 µL of 2 M hydrochloric acid was added and the solution was mixed again with a vortex mixer. The supernatant was removed and the gel was rinsed thrice with ultrapure water. To determine the loading efficiency, the amount of non-encapsulated drug in the supernatants was quantified by UV-vis spectroscopy at 303 nm and compared to a standard calibration curve of known MTX concentrations. To determine the mass of

drug loaded into the hydrogel, the total mass of non-encapsulated drug was subtracted from the initial drug mass added. The loading efficiency was calculated using the following formula:

Drug Loading Efficiency (%) = ((Mass of loaded drug)/(Mass of drug added)) x 100 (4)

To assess the drug release rate, freshly prepared MTX loaded PEI-SiNP/HA and PEI/HA hydrogels were dispersed in 1.0 mL of PBS (pH 7.4) under shaking at 37 °C. At set time points, 500 μL of the supernatant was removed and replaced with fresh PBS. The concentration of released drug in the supernatant was quantified with absorption spectroscopy at 303 nm, and the total released mass was calculated. The drug release kinetics and mechanisms were evaluated using the Korsmeyer-Peppas model:

$$F = k_m t^n \quad (5)$$

F is the fraction of released drug, the kinetic constant, k_m, describes the structural and geometric gel properties, t is the release time, and n is the release exponent dependent on the release mechanics. n was determined from the gradient of log(time) vs log(F) for the first 60 % of drug release. The kinetic constant was found by fitting eq. (5) to the release data (for $F \leq 0.6$) with the previously determined value for n.

2.13 Statistical Analysis

Results of the MTX drug loading experiments were analysed using the two-tailed Student's t-test. The differences in loading efficiencies observed between hydrogel formulations were taken to be statistically significant when $P < 0.05$.

3. Results and Discussion

3.1 Template Directed Synthesis of PEI-SiNPs

For the synthesis of the PEI-functionalised silica nanoparticles (PEI-SiNPs), a polyelectrolyte complex (PEC) templated synthesis was modified from our previously reported work[24]. Here, PECs composed of oppositely charged PEI and Glu were

prepared in a binary water-alcohol solvent and used as scaffolds for the spatio-selective hydrolysis and condensation of silanes (Figure 1A).

First, the optimal IPA concentration for the formation of PECs was determined using dynamic light scattering (DLS). As shown in Figure S1A, for IPA volume fractions below 60 % the correlation function y-intercept values were either comparable to, or less than that observed for 0 % IPA (pure water solvent) suggesting that the complex formation is purely electrostatic and no alcohol-induced assembly of PEI and Glu had occurred. A further increase in IPA to 80 – 90 % v/v led to a sharp increase to ≈ 0.85 showing an increase in signal-to-noise ratio which suggests that the alcohol induced liquid-liquid phase separation of PECs occurred. This combined with the single smooth exponential decay profiles shown in Figure S1B indicate an optimum IPA concentration for the formation of stable, monodisperse complexes. For all further experiments and PEC preparations, 80 % v/v IPA was used.

Although the complexation occurred in the presence of an excess of Glu (molar ratio of PEI to Glu monomer = 1 : 2.7), the four tertiary amines and approximately half of the three secondary amines in one monomer of PEI (pKa 11.6 and 6.7, respectively[26]) are expected to be protonated in the mixture (pH ≈ 7; Figure 2A and B). Hence, each PEI monomer will likely complex multiple Glu molecules which crosslink between PEI strands.

We next investigated the effect of PEI and Glu concentrations on the size and monodispersity of the PECs. While keeping the PEI concentration constant, the Glu concentration was systematically increased (Figure S1C). When the Glu concentration was increased from 0.2 mM to 2.2 mM, the enhanced crosslinking from larger numbers of Glu molecules decreased the PEC hydrodynamic diameter from 307.5 ± 45.5 nm to 139.2 ± 0.6 nm and the PDI from 0.24 to 0.045. In comparison, small clusters with hydrodynamic diameter of 11.4 ± 1.1 nm (PDI 0.37 ± .0.8) were observed for samples of pure PEI (without Glu).

An increase in PEI concentration from 4 to 64 µM (Glu concentration 1.09 mM) elicited a PEC diameter increase from 18.4 ± 0.1 to 153.0 ± 3.5 nm and a decrease in PDI from 0.159 to 0.042 (Figure S1D). The increase in PEI concentration to 64 µM

raised the PEI:Glu monomer ratio to 3:1, and the resultant excess of cationic groups yielded positively charged PECs with a zeta potential of 38.7 ± 1.5 mV (Figure S2). At the same time, the alkalinity of the reaction mixture was also augmented from pH 5 to 9, which is more suitable for the base-catalysed hydrolysis and condensation of silanes. Considering the size, PDI, and pH of the PECs, 1.09 mM of Glu and 64 μM of PEI were thus chosen for subsequent nanoparticle syntheses. To produce sufficient quantities for the optimisation of the nanocomposite hydrogel, the PEC formation was scaled up 25-fold while maintaining reagent concentrations and ratios. Under the scaled-up condition, the PEC size increased to 205.2 ± 4.1 nm with a PDI of 0.15.

On the addition of tetraethoxysilane (TEOS) to the PECs, silica condensation occurred inside the PEI/Glu templates to yield PEI-SiNPs with diameters of 135.5 ± 37.7 nm (by TEM) and with asymmetrical popcorn structures (Figure 1B). The hydrodynamic diameters of the PEI-SiNP were found by DLS to be 187.3 ± 4.2 nm and with a low PDI of 0.07 (Figure 1C). The broader size distribution seen by TEM was likely due to the presence of larger aggregates which arise through the clustering of particles during drying.

As shown in Figure 1D, the presentation of the PEI and its protonated tertiary amines at the particle surface conferred a positive zeta potential of 22.1 ± 1.1 mV to the PEI-SiNPs in PBS (pH 7.4). After two months of aqueous storage at room temperature, no significant change in the hydrodynamic diameter or zeta potential was observed, demonstrating the excellent colloidal stability of the PEI-SiNPs (Figure S3). The one-pot functionalisation of silica particles with branched PEI is expected to facilitate the incorporation of PEI-SiNPs into a supramolecular hydrogel with oppositely charged hyaluronic acid (HA).

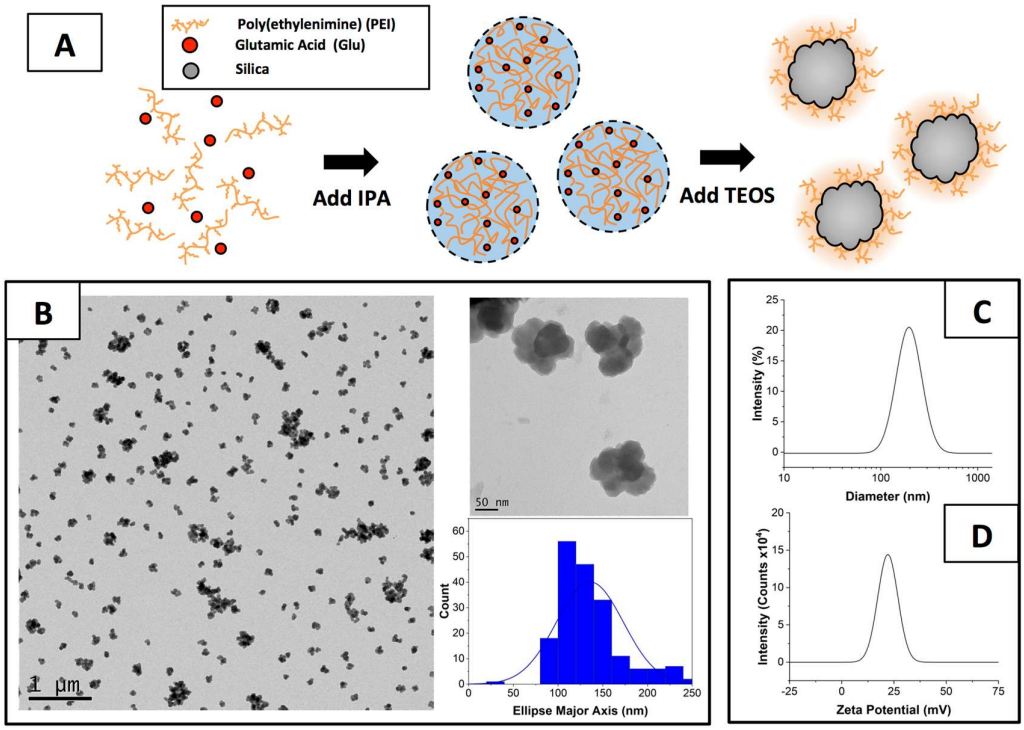

Figure 1. (A) A schematic showing the synthesis mechanism for PEI-SiNPs. (B) Representative TEM images and associated histogram of the size distribution PEI-SiNPs with an average diameter of 135.5 ± 37.7 nm (n = 188). (C) Intensity weighted size distribution collected by dynamic light scattering for PEI-SiNPs of diameter 187.3 ± 4.2 nm and PDI of 0.07 ± 0.02. (D) The zeta potential of as-synthesised particles in PBS (pH 7.4) showing a positive surface charge of 22.1 ± 1.1 mV.

The retention of PEI on the PEI-SiNP surface was further confirmed by FTIR. Within the fingerprint region, peaks for Glu and PEI were too close in wavenumber to separate in the PEI-SiNP spectra. However, the PEI spectrum shows a broad vibrational mode attributed to N-H stretching with peaks at 3382 and 3351 cm^{-1}, which occurred at 3293 and 3417 cm^{-1} for PEI-SiNPs, which were absent for Glu (Figure S4A). A PEI absorption band corresponding to CH_2 stretching at 2820 cm^{-1} was also present in the PEI-SiNP spectrum at a higher wavenumber of 2854 cm^{-1} but not in Glu [27,28].

TGA analysis was used as a complementary technique to confirm the retention of Glu and PEI within the synthesised PEI-SiNPs. As shown in Figure S4B, the initial weight loss for PEI-SiNPs at ~ 200 °C can be attributed to the decomposition of Glu. Pristine

Glu shows a first derivative peak at comparable temperatures (onset of 191 °C) and no PEI degradation is observed until 310 °C. Above this, the Glu and PEI weight loss profiles overlap to give the profile observed for the PEI-SiNPs.

3.2 Formation of PEI-SiNP/HA and PEI/HA Coacervate Hydrogels

Hyaluronic acid (HA), a non-sulfated glycosaminoglycan and extracellular matrix component, exhibits excellent biocompatibility, non-immunogenicity, and biodegradability[29]. As it is negatively charged at physiological pH, HA was used to electrostatically complex with cationic PEI-SiNPs to obtain PEI-SiNP/HA nanocomposite hydrogels.

During the initial mixing of PEI-SiNPs and HA, the alkaline environment (pH ~10) induced a low degree of protonation of PEI's primary, secondary, and tertiary amines (pKa 4.5, 6.7, and 11.6, respectively), hence resulting in the formation of a white precipitate following charge neutralisation by the $-COO^-$ groups present in HA (Figure 2C). Upon pH adjustment to ~6 with hydrochloric acid, a greater degree of protonation of PEI's tertiary and secondary amines was achieved. The enhanced electrostatic interaction between PEI and HA resulted in the formation of a complex coacervate hydrogel along with contraction of the polymeric networks during syneresis. This process resulted in the formation of an opaque white hydrogel suspended in a colourless liquid (Figure 2D). It is important to note that when PEI-SiNPs were replaced with negatively charged non-PEI functionalised SiNPs of comparable size that were synthesised using our previously reported protocol (Figure S5A and S5B),[24] no gelation between the SiNPs and HA was observed (Figure S5C). This result clearly demonstrates that the electrostatic interactions between the oppositely charged PEI-SiNP and HA are critical in the gelation process.

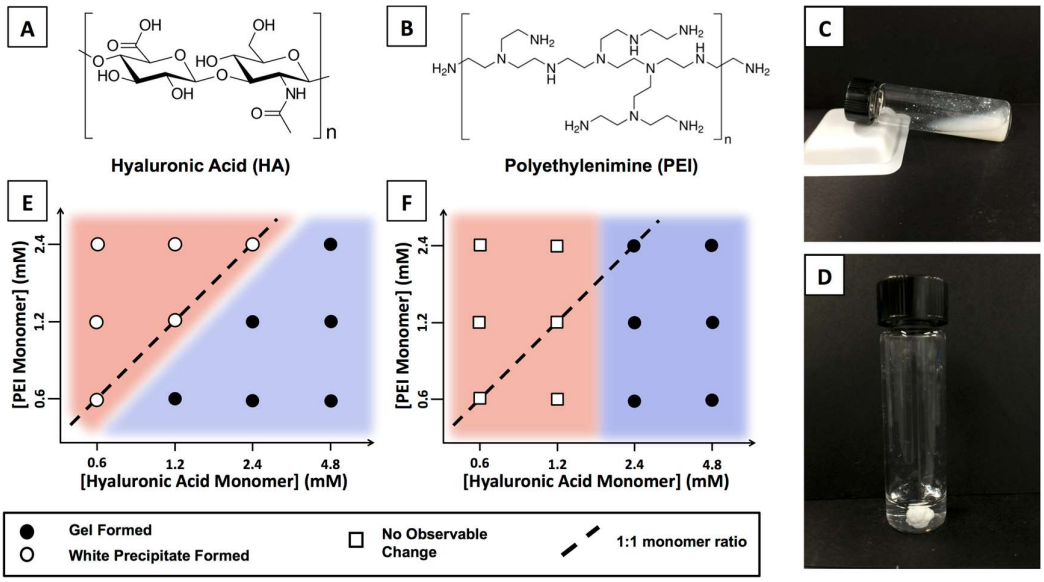

Figure 2. Chemical structures of (A) hyaluronic acid (HA) and (B) polyethylenimine (PEI). Photographs of taken during PEI-SiNP/HA hydrogel synthesis showing (C) the white precipitates formed after the initial mixing of PEI-SiNPs and HA, and (D) the coacervate hydrogel formed in a colourless supernatant after reduction of the pH and resultant syneresis. Schematics showing the gel forming conditions for (E) PEI-SiNP/HA gels, and (F) PEI/HA gels.

As the driving force for gelation is electrostatic interactions between the ionisable groups of PEI and HA, the effect of their concentrations and charge stoichiometry was investigated. For all PEI-SiNP/HA samples with a PEI:HA monomer ratio ≤ 1:1, hydrogels formed instantaneously on mixing after pH reduction (Figure 2E). At the final pH of ~6, each HA monomer possesses one anionic carboxyl group (pKa 3.0[30]; Figure 2A) and each PEI monomer has seven cationic secondary and tertiary amines (pKa 6.7 and 11.6 respectively; Figure 2B), hence each PEI monomer is likely to complex several HA monomers. For PEI:HA monomer ratios ≥ 1:1 however, phase separation and bulk gelation did not occur clearly demonstrating that on average each PEI monomer must complex with more than one HA monomer for hydrogel formation.

When gels were formed with pristine PEI in place of PEI-SiNPs, the gelation occurred independent of PEI/HA monomer stoichiometry and was more dependent on

the concentration of HA. A minimum HA monomer concentration of 2.4 mM was found to be critical for gelation for all PEI concentrations tested (Figure 2F). Notably, the total amount of PEI and HA required to induce gelation was found to be lower for the PEI-SiNP/HA compared to PEI/HA samples. Taken together, it is evident that the conjugation of PEI to the silica particle surface significantly affects the network crosslinking mechanics in electrostatic-mediated gelation, and as will be shown in the following discussion, yields gels with notably different physical properties.

The amount of PEI and HA incorporated into the PEI-SiNPs/HA hydrogels was estimated by quantifying the concentrations remaining in the expelled liquid following syneresis. With the HA monomer concentration fixed at 4.8 mM, increasing the concentration of SiNP-bound PEI from 0.6 to 3.6 mM led to an increase in the amount of PEI-SiNP and HA incorporated in the hydrogel as the concentration of PEI-SiNP and HA present in the supernatant decreased by 12 % and 10 % relative to the added dose (Figure S6A and B). A similar trend was observed when HA was increased from 1.2 to 4.8 mM with PEI fixed at 0.6 mM. With increasing HA, a higher amount of PEI-SiNP was incorporated into the hydrogel whereas the amount of HA incorporated remained high with no significant change across the samples (Figure S6C & D). Although a similar trend in which an increased relative incorporation of PEI and HA into the hydrogels was observed for the PEI/HA hydrogels, the total amount of both components present in the hydrogel was lower than the PEI-SiNP/HA hydrogels. These results suggest that the use of PEI-SiNP as multifunctional crosslinkers could lead to an increased local charge density on the surface of the SiNPs to enhance electrostatic interactions with HA in the complex coacervates, hence resulting in an increased incorporation of PEI-SiNPs and HA into the hydrogel.

3.3 The Effect of PEI-SiNP Incorporation on Nanocomposite Hydrogel Morphology

As the pore morphology of hydrogels could greatly influence their mechanical properties and drug release kinetics, cryo-SEM, which enables preservation of the hydrated state of the hydrogel, was used to study the microstructural features of the PEI-SiNP/HA nanocomposite hydrogel.

As is shown in Figure 3A and B, HA only samples possessed a highly porous network structure with thin walls. In contrast, the electrostatic interactions of PEI with HA in the PEI/HA hydrogels resulted in the formation of denser walls between adjacent pores (Figure 3C & D). The network structure was also comparatively heterogeneous, showing a wide range of pore sizes and wall thicknesses compared to the HA only sample. With the PEI-SiNP/HA hydrogel, a significant change in network structure occurred. Unlike the smooth continuous walls with typical thickness of < 1 μm seen with the PEI/HA hydrogels, thick walls of densely packed and homogeneously dispersed PEI-SiNPs with widths up to several microns were observed for the PEI-SiNP/HA hydrogels (Figure 3E & F). The micron-scale pores between the walls present in the PEI-SiNP/HA hydrogels also show a larger diameter (approximately 5 μm) and reduced inter-connectivity compared to the PEI/HA hydrogel (pore diameter of approximately 0.5 – 2.5 μm). Furthermore, the PEI-SiNP packing in the case of PEI-SiNP/HA nanocomposite hydrogel gives rise to a secondary nanoscale pore network spanning the meso- and macro-porous range.

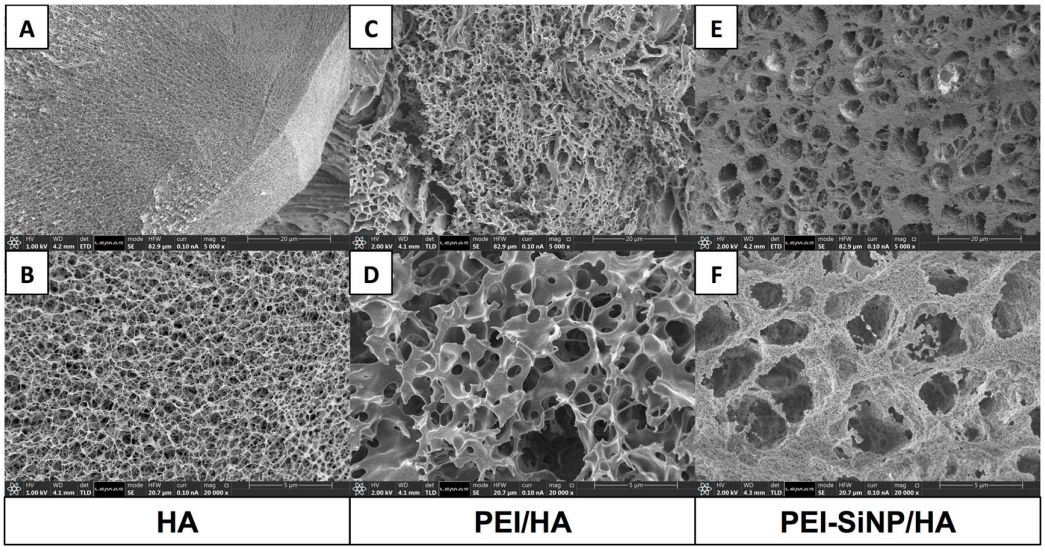

Figure 3. The effect of PEI-SiNP incorporation on the structure and morphology of hydrogels. Cryo-SEM images of (A, B) HA only, (C, D) PEI/HA, and (E, F) PEI-SiNP/HA hydrogels prepared with PEI/HA monomer ratio of 3.6/4.8. The scale bars represent 20 μm (A, C, E) and 5 μm (B, D, F).

3.4 Equilibrium Swelling Ratio of Nanocomposite Hydrogels

To evaluate their swelling ratio, the mass of the freshly prepared hydrogel was compared to that obtained after complete drying under mild conditions. As seen in Figure S7, comparable swelling ratios were observed for both hydrogel types and the changes in gelator ratios had no significant effect on the degree of swelling. The modest decrease in swelling observed on the incorporation of PEI-SiNPs is likely caused by the high concentration of SiNPs (shown in Figure 3F) and corresponding high mass density of the hydrogel relative to the PEI/HA networks which manifests as a lower (mass normalised) swelling ratio.

The swelling ratios presented herein exceeded that of comparable SiNP nanocomposite hydrogels synthesised with dynamic covalent crosslinks[15,17], but were significantly lower than those typically reported for physical nanocomposites. For example, in-*situ* grafted poly(acrylic acid)-functionalised SiNPs with hydrogen bond crosslinks were shown to have swelling ratios in excess of 10,000 %[8,31]. The lower swelling ratios observed with polyelectrolyte hydrogels could be attributed to the stronger electrostatic interactions within the polymeric networks compared to weaker bonds such as hydrogen bonding.[32–34]

3.5 Rheological Characterisation of PEI-SiNP/HA and PEI/HA Hydrogels

It is known that a mismatch in mechanical stiffness can cause poor apposition between hydrogels and the surrounding tissues leading to poor drug diffusion, and a decrease in efficacy. While very weak hydrogels may experience poor interfacing with the tissue walls and premature degradation in dynamic biological environments, excessive stiffness can cause mechano-chemical injuries and foreign body reactions.[35,36] As such, the ability to achieve controllable and tuneable stiffness is highly desirable for the biological application of hydrogels. The viscoelastic behaviour of the hydrogels was confirmed with a frequency sweep at 1 % strain which displayed significantly higher values of G' than G" between 0.1 and 10 Hz for both PEI-SiNP/HA and PEI/HA (Figure S8A). As seen in Figure 4A, the PEI-SiNP/HA hydrogels prepared at various PEI:HA ratios displayed much higher

mechanical stiffness than the PEI/HA hydrogels, which could be attributed to the multifunctional crosslinking and high density packing of the organic-inorganic hybrid PEI-SiNPs (Figure 3F). In addition, the conjugation of branched PEI to the SiNP surface may lead to reduced molecular motion and enhanced local charge densities for stronger electrostatic crosslinking with the polyanionic HA.

The incorporation of PEI-SiNP with HA also decreases the energy dissipation potential as shown by the lower loss factor (tan δ) obtained for most of the PEI-SiNP/HA nanocomposite hydrogels (Figure S8B). In the PEI/HA hydrogels, the presence of relatively weak, purely physical crosslinks in the polymer network allows for energy dissipation through the reversible breaking of electrostatic bonds and resultant structural rearrangement. In the PEI-SiNP/HA hydrogels, however, the covalent bonds between PEI and the SiNPs do not reversibly break, which decreases the networks' ability to dissipate energy through structural reconfiguration and induces network elasticity. Yang *et al.* also observed a similar relationship with hydrogels formed from hydrogen bonding between poly(acrylamide)-functionalised SiNPs where higher concentrations of silica decreased the loss factor compared to polymer-only hydrogels.[37]

As the charge ratio between oppositely charged polymers in electrostatically crosslinked hydrogels is expected to modulate the mechanical properties,[38] the molar ratio of PEI to HA monomers was systematically varied to study tuneability in the hydrogel stiffness. A reduction in PEI monomer and hence PEI-SiNP concentrations from 3.6 to 1.2 mM led to a stepwise increase in the storage moduli of the PEI-SiNP/HA hydrogels from 3,276 Pa to 10,617 Pa. The reduction of excess cationic charges (Table 1) could have resulted in decreased electrostatic repulsions between the incorporated PEI-SiNPs which led to stronger interactions with the polyanionic HA in the hydrogel network. A further decrease in the PEI monomer concentration to 0.6 mM, however, led to a marked decrease in hydrogel stiffness. This could be attributed to a weakened hydrogel network due to reduced availability of PEI-SiNPs to electrostatically crosslink with HA, along with increased repulsion between the HA chains. The same trend was observed for PEI/HA where the stiffest network was observed at PEI:HA monomer ratio of 1.2:4.8. The tuneable variation of the storage

modulus shows that the hydrogel composition may be specifically chosen to match that of the target tissues.

Table 1. Cation:Anion charge ratios present in PEI-SiNP/HA and PEI/HA hydrogels prepared at differing PEI/HA monomer ratios.

PEI/HA Monomer Ratio	3.6/4.8	2.4/4.8	1.2/4.8	0.6/4.8
Cation:Anion Charge Ratio	4.8:1	3.2:1	1.6:1	0.8:1

Following implantation in the body, the dynamic biological environment and tissue remodelling could subject the hydrogel to strain, causing network breakage and treatment failure for a hydrogel with insufficient critical strain value[39,40]. As seen from Figure 4B, strain sweeps revealed that the electrostatic crosslinking of PEI-SiNPs maintained the viscoelastic properties of PEI-SiNP/HA up to a much higher shear strain compared to that for PEI/HA hydrogels (304 % *vs.* 46.9 %). These results suggest that the PEI-SiNP/HA nanocomposite hydrogels are more likely to retain their physical properties following *in vivo* application.

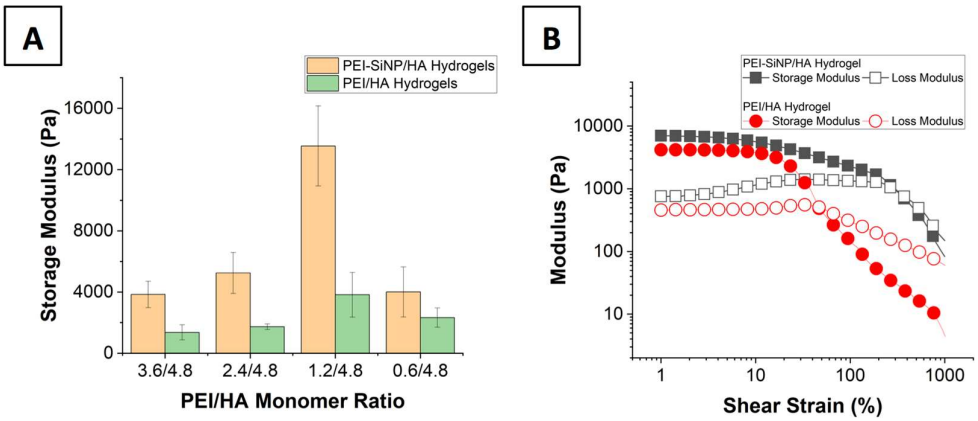

Figure 4. (A) The storage moduli measured at 1 % shear strain and a frequency of 1 Hz for PEI-SiNP/HA and PEI/HA hydrogels prepared at different PEI/HA monomer ratios (n = 3). (B) A strain sweep for PEI-SiNP/HA and PEI/HA hydrogels (PEI/HA monomer ratio 1.2/4.8) at a frequency of 1 Hz.

3.6 Thixotropy and Self-Healing

The ability of physical hydrogels to undergo shear thinning aids in their injection or application to the body whilst the recovery of networks upon removal of the shear stress enables their mechanical properties to be restored for the intended purpose. When subject to large shear strains (1000 % strain) the reversible breakage of the physical crosslinks between PEI-SiNPs and HA resulted in a 100-fold decrease in mechanical stiffness and increased flow (G' < G"; Figure 5A). Reformation of the electrostatic bonds and recovery of the viscoelastic properties occurred almost instantaneously on return to a low shear strain regime (1 % strain). This result is consistent with other reported studies. For example, Arno *et al.* observed a reversible ~100x decrease in G' for electrostatic calcium-alginate hydrogels reinforced with poly(L-lactide)-based nanoparticles under high mechanical strain[41]. Similarly, Zhang and co-workers also observed a decrease in stiffness by an order of magnitude for the chitosan-strengthened polyacrylamide-based guest-host hydrogel under high strain, which subsequently recovered within seconds of return to the low strain regime[42]. Interestingly, after the high-strain cycle used in our study, the storage modulus of the nanocomposite hydrogel only partially recovered to 7.5 kPa (initial G' = 9.6 kPa) in the low strain period. This behaviour suggests that while initial recovery and reformation of the physical crosslinks may occur within seconds, the structural reorganisation required for complete stiffness recovery may take longer than the 30 s afforded in the 1 % shear strain cycle in this experiment.

To assess the self-healing properties of the PEI-SiNP/HA hydrogels, two pieces of hydrogel (one strained blue with CBBG dye) were cut in half and placed in intimate contact (Figure 5B). After incubation at room temperature for 1 h the hydrogels had joined at their interface, could support their own weight, and remained attached under mechanical stretching (Figure 5C & D).

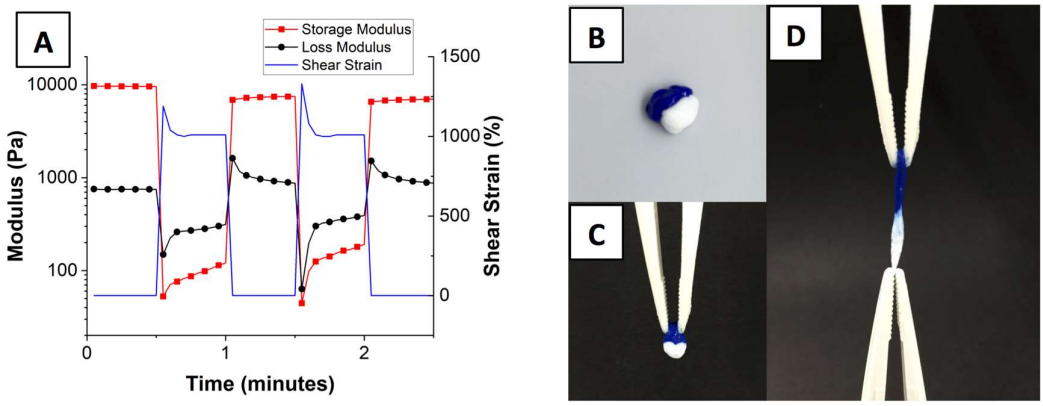

Figure 5. (A) The storage modulus for PEI-SiNP/HA hydrogels (PEI/HA monomer ratio 1.2:4.8; measurement frequency 1 Hz) under repeated cycles of 1 % and then 1000 % strain (interval time 30 s). (B) Two pieces of hydrogel, prepared with and without CBBG dye, cut in half, and placed in intimate contact to demonstrate their macroscopic self-healing properties. After 1 h the hydrogels support their own weight (C) and remain connected under mild mechanical stretching (D).

3.7 Haemolytic Activity and Cytotoxicity of PEI-SiNP/HA Hydrogels

The haemocompatibility of the PEI-SiNP/HA nanocomposite hydrogels was evaluated using mouse mammalian blood. As seen in Figure 6A, minimal hemolysis (≤ 3.8%) was observed for the PEI-SiNP/HA and PEI/HA hydrogels, hence demonstrating good haemocompatibility. In contrast, free PEI and PEI-SiNPs induced significant haemolysis over a similar concentration range (PEI monomer concentrations of 0.37 – 2.2 mM; Figure 6B and 6C). As expected, HA, a naturally occurring component of the extracellular matrix, showed negligible haemolysis over the concentration range used in hydrogel preparation (< 2.6%; HA monomer concentrations of 0.73 – 2.9 mM; Figure 6D). These results clearly demonstrate that the charge screening and electrostatic complexation of high molecular weight PEI by the oppositely charged HA polymer could mitigate the haemotoxicity of the resultant hydrogel. In addition, the PEI-SiNP/HA hydrogels were also found to induce minimal cytotoxicity in RAW264.7 and HCT116 cells (Figure S9). Such charge balanced hydrogels thus offer an advantage over conventional PEI-containing hydrogels which tend to be cytotoxic due to the disruption of mammalian cell membranes by PEI's high cationic charged densities[43,44].

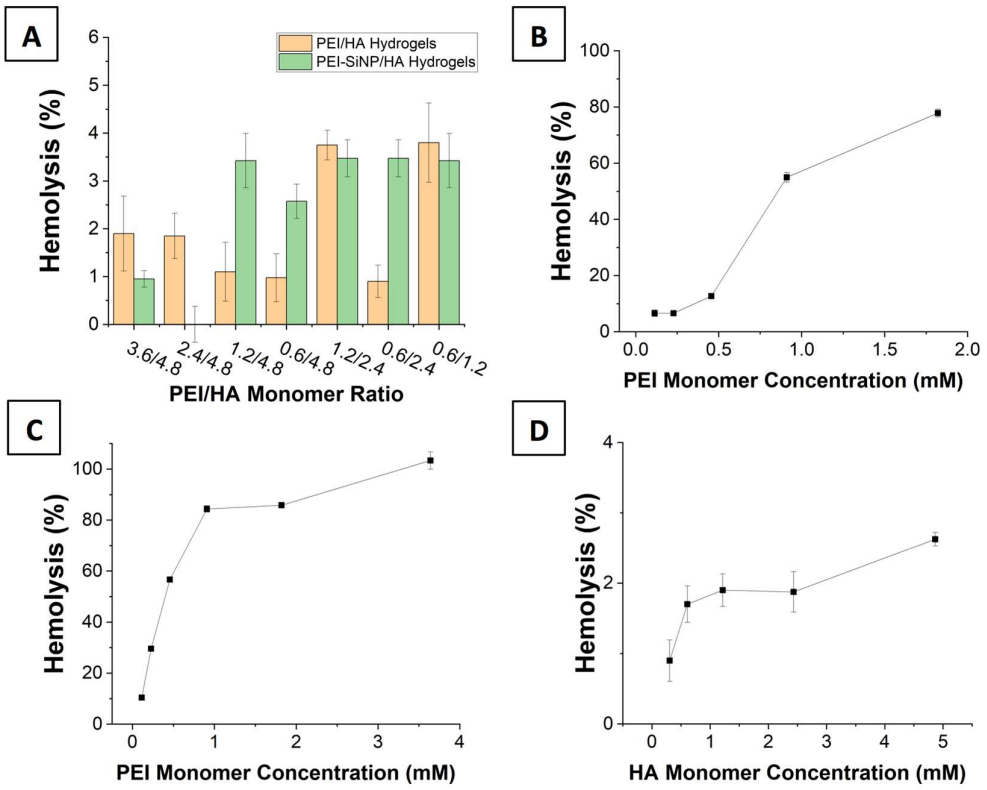

Figure 6. Haemolysis testing for (A) PEI-SiNP/HA and PEI/HA hydrogels, and (B-D) PEI, PEI-SiNPs, and HA respectively. Data are expressed as mean ± standard deviations of 4 replicates.

3.8 Methotrexate Drug Loading and Release

Abraham *et al.* recently demonstrated that electrostatic interactions between oppositely charged cargoes and supramolecular hydrogel networks can retard cargo release[45]. As discussed in Section 3.1, the presence of protonated amines in the silica surface-bound PEI conferred a positive surface charge. Because of the large number of ionisable groups per PEI monomer (7 protonated amines per PEI monomer vs 1 deprotonated carboxyl group per HA monomer at pH 7.4), an excess of cationic groups is still expected to be available for electrostatic interaction with a guest molecule after hydrogel formation. As such, we investigated the loading and release of an oppositely charged cargo. MTX, an anti-metabolite of folic acid, is used as an anticancer agent in the treatment of a variety of neoplasms.[46] However, the drug efficacy is limited by its poor pharmacokinetic properties including rapid renal

clearance, short plasma half-life, and low tumour accumulation following conventional administration by injection or oral routes.[47] Furthermore, the use of MTX is associated with dose-limiting systemic toxicities such as hepatotoxicity and bone marrow suppression. Owing to its two ionisable carboxyl groups that carry a negative charge at physiological pH, MTX was incorporated into the PEI-SiNP/HA hydrogel via electrostatic interaction with the cationic PEI-SiNPs prior to the addition of HA. The implantation of the MTX loaded PEI-SiNP/HA hydrogel could allow for direct delivery of the anticancer drug to the tumour site, hence reducing systemic toxicities and increasing drug bioavailability to the tumour.

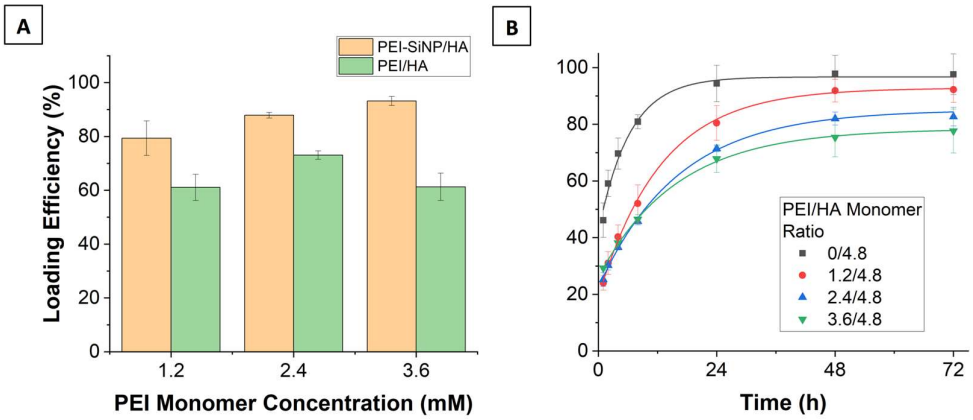

Figure 7. (A) MTX loading efficiencies for PEI-SiNP/HA and Free-PEI/HA gels (n=3). (B) Cumulative drug release from PEI-SiNP/HA hydrogels collected in pH 7.4 PBS at 37 °C (n = 3).

As shown in Figure 7A, a significantly higher MTX loading efficiency was observed for the PEI-SiNP/HA compared to PEI/HA hydrogels ($P < 0.05$ for all). Interestingly, the loading of MTX into the PEI-SiNP/HA nanocomposite hydrogels was found to be dependent on the ratio of PEI to HA. When the PEI monomer concentration (and hence PEI-SiNPs) was increased from 1.2 to 3.6 mM, the MTX loading efficiency increased from 79 to a maximum at 93%. This result is consistent with the expected increase in availability of protonated amines for electrostatic complexation with MTX as the PEI concentration increases.

690 The drug release profiles and kinetics for the PEI-SiNP/HA nanocomposite hydrogels
691 were next evaluated with the Korsemeyer-Peppas model[48]. As seen from Figure 7B, a
692 slower, more sustained, and tuneable drug release was observed for the PEI-SiNP/HA
693 compared to the HA only hydrogel. The HA only hydrogel showed a rapid burst
694 release with > 80% of MTX released within 8 h, and almost 100 % released by 24 h.
695 In contrast, electrostatic interactions between MTX and the PEI-SiNPs resulted in a
696 much slower drug release from the PEI-SiNP/HA hydrogels. For example, the
697 hydrogel prepared with a 3.6/4.8 PEI/HA monomer ratio gave a 47 % MTX release
698 after 8 h, 68 % drug release at 24 h, followed by a more gradual increase in drug
699 release up to 72 h. The kinetic constant, k_m, observed with the HA only hydrogel was
700 considerably higher that of the nanocomposite hydrogels (Table 2). Interestingly, the
701 MTX release up to 8 h was approximately comparable for the nanocomposite
702 hydrogels. Beyond this time, the rate of drug release decreased with the amount of
703 PEI-SiNP present within the nanocomposite hydrogel. With nanocomposite hydrogels
704 containing PEI/HA monomer ratios of 1.2/4.8, 91% of the loaded MTX mass was
705 released over 72 h; this decreased to 83% and 78% for the 2.4/4.8 and 3.6/4.8 ratios,
706 respectively. The initial drug release profile up to 8 h could possibly be due to the
707 desorption and diffusion of electrostatically bound MTX from the wall surfaces of the
708 hydrogel pores, which were found to be considerably larger than the size of MTX (as
709 discussed in Section 3.3).[49] Beyond this time, the MTX contained on the pore surfaces
710 was depleted, and the remaining anionic drug was complexed with the cationic PEI-
711 SiNPs inside the hydrogel walls. Electrostatic interactions were greater in the
712 hydrogels prepared with higher PEI-SiNP concentrations, which retarded the transit of
713 MTX from inside the walls into the pore spaces and out of the hydrogel.
714
715 Taken together, these results clearly demonstrate the ability to modulate the release of
716 the anionic anticancer drug MTX by varying PEI-PSiNP concentration within the
717 nanocomposite hydrogels. Importantly, the electrostatic complexation of PEI-PSiNP
718 with HA to form the nanocomposite hydrogel avoids the near complete burst release
719 observed with the HA only hydrogel. For all samples, the exponent n was < 0.5
720 suggesting that diffusion was controlled by fickian diffusion of the guest molecule
721 from within the hydrogel matrix rather than hydrogel swelling or dissolution.
722

Table 2. The release exponent, n, and kinetic constant, k_m, derived from the Korsmeyer-Peppas model, and R^2 values from the fitting for the drug release profiles presented in Figure 7B.

Gel Condition	n	k_m	R^2
PEI-SiNP/HA – 0/4.8	0.26	47.8	0.990
PEI-SiNP/HA – 1.2/4.8	0.38	23.8	0.999
PEI-SiNP/HA – 2.4/4.8	0.31	23.9	0.995
PEI-SiNP/HA – 3.6/4.8	0.22	29.2	0.986

4. Conclusion

In this study, we have developed a facile protocol for the one-pot synthesis of organic-inorganic hybrid PEI-SiNPs using PEI/Glu PECs as templates for spatio-selective silane mineralisation. The core-shell PEI-SiNP can be used to electrostatically complex with polyanionic HA to form complex coacervate-based nanocomposite hydrogel. Due to the reversible electrostatic bonding between PEI-SiNP and HA, the nanocomposite hydrogels possessed desirable shear-thinning and self-healing properties. Furthermore, the incorporation of the hybrid organic-inorganic PEI-SiNPs enhanced the mechanical stiffness of the nanocomposite hydrogels compared to the PEI/HA hydrogels. The mechanical stiffness of the nanocomposite hydrogels could also be readily tailored through tuning the ratio of PEI-SiNP to HA.

It was also found that the electrostatic complexation of PEI-SiNPs with HA could mitigate the cytotoxicity concerns traditionally associated with high molecular weight PEI thus improving their suitability for biological applications. The modular approach used also offers benefit over *in-situ* polymerised SiNP-nanocomposite hydrogels that use potentially cytotoxic reagents[7,18,50,51]. Finally, we exploited the excess cationic charges present to enhance the loading and retard the release anionic anti-cancer therapeutic MTX. In conclusion, the novel synthetic pathway presented herein affords improved mechanical stiffness, self-healing, as well as enhanced drug loading and release capability while offering greater simplicity and biocompatibility over

currently established protocols for the construction of nanocomposite hydrogels for biomedical applications.

CRediT Authorship Contribution Statement

George Newham: Conceptualization, Methodology, Investigation, Formal Analysis, Writing – original draft. **Stephen D. Evans**: Supervision, Writing – review & editing. **Zhan Yuin Ong**: Conceptualization, Methodology, Supervision, Writing – review & editing, Funding acquisition.

Supporting Information

The following files are available free of charge. Experimental methods for the preparation of PEI/Glu PECs and the synthesis of SiNPs without PEI surface funcitonality; DLS data for PEI/Glu PECs including correlation function curves at varied solvent alcohol concentration and size characterisation with PEI an Glu concentration variation; TGA and FTIR data for PEI, Glu, and PEI-SiNPs; size and zeta potential characterisation for SiNPs without surface PEI, and photographs of their unsuccessful gelation with HA; quantification of the concentrations of HA and PEI present in the hydrogel supernatants after gelation; and additional rheology data including frequency sweeps and loss factor data for PEI-SiNP/HA and PEI/HA hydrogels (PDF). The raw experimental dataset obtained from this study is available to download from doi.org/10.5518/1060.

Acknowledgements

This work was supported by the Engineering and Physical Sciences Research Council (EPSRC; EP/V009516/1). G.N. acknowledges support from the University of Leeds and EPSRC DTP for a PhD studentship. S.D.E. acknowledges support from the EPSRC (EP/P023266/1) and National Institute for Health Research infrastructure, at Leeds. We also thank the Leeds Electron Microscopy and Spectroscopy Centre (LEMAS) for their assistance in the collection of cryo-SEM images, Dr. Matthew Hughes (University of Leeds) for his assistance in rheological characterisation, and Dr. Nicola Ingram for the collection of mouse blood.

Abbreviations

SiNP	Silica Nanoparticle
PEI	Polyethylenimine
HA	Hyaluronic Acid
PEI-SiNP	Polyethylenimine Functionalised Silica Nanoparticle
PEC	Polyelectolyte Complex
Glu	Glutamic Acid
MTX	Methotrexate
CTAB	Cetrimonium Bromide
PAA	Poly(acrylic acid)
Arg	L-Arginine
TEOS	Tetraethoxysilane
CBBG	Coomassie Brilliant Blue
IPA	2-Isopropanol
DLS	Dynamic Light Scattering
TEM	Transmission Electron Microscopy
SEM	Scanning Electron Microscopy
TGA	Thermogravimetric Analysis
FTIR	Fourier Transform Infrared Spectroscopy

References

(1) Talebian, S.; Mehrali, M.; Taebnia, N.; Pennisi, C. P.; Kadumudi, F. B.; Foroughi, J.; Hasany, M.; Nikkhah, M.; Akbari, M.; Orive, G.; Dolatshahi-Pirouz, A. Self-Healing Hydrogels: The Next Paradigm Shift in Tissue Engineering? *Adv. Sci.* **2019**, *6* (16). https://doi.org/10.1002/advs.201801664.

(2) Xiong, Y.; Zhang, X.; Ma, X.; Wang, W.; Yan, F.; Zhao, X.; Chu, X.; Xu, W.; Sun, C. A Review of the Properties and Applications of Bioadhesive Hydrogels. *Polym. Chem.* **2021**, *12* (26), 3721–3739. https://doi.org/10.1039/d1py00282a.

(3) Li, J.; Mooney, D. J. Designing Hydrogels for Controlled Drug Delivery. *Nat. Rev. Mater.* **2016**, *1* (12). https://doi.org/10.1038/natrevmats.2016.71.

(4) Li, W.; Feng, R.; Wang, R.; Li, D.; Jiang, W.; Liu, H.; Guo, Z.; Serpe, M. J.; Hu, L. Polyelectrolyte-Based Physical Adhesive Hydrogels with Excellent Mechanical Properties for Biomedical Applications. *J. Mater. Chem. B* **2018**, *6*

(29), 4799–4807. https://doi.org/10.1039/c8tb01160e.

(5) Zeimaran, E.; Pourshahrestani, S.; Fathi, A.; Razak, N. A. bin A.; Kadri, N. A.; Sheikhi, A.; Baino, F. Advances in Bioactive Glass-Containing Injectable Hydrogel Biomaterials for Tissue Regeneration. *Acta Biomater.* **2021**. https://doi.org/10.1016/j.actbio.2021.09.034.

(6) Zheng, J.; Xiao, P.; Liu, W.; Zhang, J.; Huang, Y.; Chen, T. Mechanical Robust and Self-Healable Supramolecular Hydrogel. *Macromol. Rapid Commun.* **2016**, *37* (3), 265–270. https://doi.org/10.1002/marc.201500571.

(7) Shi, F.-K.; Wang, X.-P.; Guo, R.-H.; Zhong, M.; Xie, X.-M. Highly Stretchable and Super Tough Nanocomposite Physical Hydrogels Facilitated by the Coupling of Intermolecular Hydrogen Bonds and Analogous Chemical Crosslinking of Nanoparticles. *J. Mater. Chem. B* **2015**, *3* (7), 1187–1192. https://doi.org/10.1039/C4TB01654H.

(8) Yang, J.; Han, C. R.; Duan, J. F.; Xu, F.; Sun, R. C. Insitu Grafting Silica Nanoparticles Reinforced Nanocomposite Hydrogels. *Nanoscale* **2013**, *5* (22), 10858–10863. https://doi.org/10.1039/c3nr04252a.

(9) Wu, C.; Wang, C.; Sun, L.; Xu, K.; Zhong, W. PLGA Nanoparticle-Reinforced Supramolecular Peptide Hydrogels for Local Delivery of Multiple Drugs with Enhanced Synergism. *Soft Matter* **2020**, *16* (46), 10528–10536. https://doi.org/10.1039/d0sm01152e.

(10) Yu, J.; Ha, W.; Sun, J. N.; Shi, Y. P. Supramolecular Hybrid Hydrogel Based on Host-Guest Interaction and Its Application in Drug Delivery. *ACS Appl. Mater. Interfaces* **2014**, *6* (22), 19544–19551. https://doi.org/10.1021/am505649q.

(11) Wu, H.; Song, L.; Chen, L.; Zhang, W.; Chen, Y.; Zang, F.; Chen, H.; Ma, M.; Gu, N.; Zhang, Y. Injectable Magnetic Supramolecular Hydrogel with Magnetocaloric Liquid-Conformal Property Prevents Post-Operative Recurrence in a Breast Cancer Model. *Acta Biomater.* **2018**, *74*, 302–311. https://doi.org/10.1016/j.actbio.2018.04.052.

(12) Mihajlovic, M.; Mihajlovic, M.; Dankers, P. Y. W.; Masereeuw, R.; Sijbesma, R. P. Carbon Nanotube Reinforced Supramolecular Hydrogels for Bioapplications. *Macromol. Biosci.* **2019**, *19* (1). https://doi.org/10.1002/mabi.201800173.

(13) Yang, J.; Shi, F. K.; Gong, C.; Xie, X. M. Dual Cross-Linked Networks

Hydrogels with Unique Swelling Behavior and High Mechanical Strength: Based on Silica Nanoparticle and Hydrophobic Association. *J. Colloid Interface Sci.* **2012**, *381* (1), 107–115. https://doi.org/10.1016/j.jcis.2012.05.046.

(14) Yang, J.; Gong, C.; Shi, F. K.; Xie, X. M. High Strength of Physical Hydrogels Based on Poly(Acrylic Acid)-g-Poly(Ethylene Glycol) Methyl Ether: Role of Chain Architecture on Hydrogel Properties. *J. Phys. Chem. B* **2012**, *116* (39), 12038–12047. https://doi.org/10.1021/jp303710d.

(15) Wu, M.; Chen, J.; Huang, W.; Yan, B.; Peng, Q.; Liu, J.; Chen, L.; Zeng, H. Injectable and Self-Healing Nanocomposite Hydrogels with Ultrasensitive PH-Responsiveness and Tunable Mechanical Properties: Implications for Controlled Drug Delivery. *Biomacromolecules* **2020**, *21* (6), 2409–2420. https://doi.org/10.1021/acs.biomac.0c00347.

(16) Zhang, C.; Liang, K.; Zhou, D.; Yang, H.; Liu, X.; Yin, X.; Xu, W.; Zhou, Y.; Xiao, P. High-Performance Photopolymerized Poly(Vinyl Alcohol)/Silica Nanocomposite Hydrogels with Enhanced Cell Adhesion. *ACS Appl. Mater. Interfaces* **2018**, *10* (33), 27692–27700. https://doi.org/10.1021/acsami.8b09026.

(17) Zengin, A.; Castro, J. P. O.; Habibovic, P.; van Rijt, S. H. Injectable, Self-Healing Mesoporous Silica Nanocomposite Hydrogels with Improved Mechanical Properties. *Nanoscale* **2021**, *13* (2), 1144–1154. https://doi.org/10.1039/D0NR07406C.

(18) Zhong, M.; Liu, X. Y.; Shi, F. K.; Zhang, L. Q.; Wang, X. P.; Cheetham, A. G.; Cui, H.; Xie, X. M. Self-Healable, Tough and Highly Stretchable Ionic Nanocomposite Physical Hydrogels. *Soft Matter* **2015**, *11* (21), 4235–4241. https://doi.org/10.1039/c5sm00493d.

(19) Yang, J.; Wang, X. P.; Xie, X. M. In Situ Synthesis of Poly(Acrylic Acid) Physical Hydrogels from Silica Nanoparticles. *Soft Matter* **2012**, *8* (4), 1058–1063. https://doi.org/10.1039/c1sm06647a.

(20) Shi, F. K.; Zhong, M.; Zhang, L. Q.; Liu, X. Y.; Xie, X. M. Robust and Self-Healable Nanocomposite Physical Hydrogel Facilitated by the Synergy of Ternary Crosslinking Points in a Single Network. *J. Mater. Chem. B* **2016**, *4* (37), 6221–6227. https://doi.org/10.1039/c6tb01606e.

(21) Alvarez, G. S.; Hélary, C.; Mebert, A. M.; Wang, X.; Coradin, T.; Desimone,

M. F. Antibiotic-Loaded Silica Nanoparticle-Collagen Composite Hydrogels with Prolonged Antimicrobial Activity for Wound Infection Prevention. *J. Mater. Chem. B* **2014**, *2* (29), 4660–4670. https://doi.org/10.1039/c4tb00327f.

(22) Shi, Y.; Hélary, C.; Coradin, T. Exploring the Cell–Protein–Mineral Interfaces: Interplay of Silica (Nano)Rods@collagen Biocomposites with Human Dermal Fibroblasts. *Mater. Today Bio* **2019**, *1* (April), 1–10. https://doi.org/10.1016/j.mtbio.2019.100004.

(23) Adibnia, V.; Taghavi, S. M.; Hill, R. J. Roles of Chemical and Physical Crosslinking on the Rheological Properties of Silica-Doped Polyacrylamide Hydrogels. *Rheol. Acta* **2017**, *56* (2), 123–134. https://doi.org/10.1007/s00397-016-0989-5.

(24) Newham, G.; Mathew, R. K.; Wurdak, H.; Evans, S. D.; Ong, Z. Y. Polyelectrolyte Complex Templated Synthesis of Monodisperse, Sub-100 Nm Porous Silica Nanoparticles for Cancer Targeted and Stimuli-Responsive Drug Delivery. *J. Colloid Interface Sci.* **2021**, *584*, 669–683. https://doi.org/10.1016/j.jcis.2020.10.133.

(25) Oueslati, N.; Leblanc, P.; Harscoat-Schiavo, C.; Rondags, E.; Meunier, S.; Kapel, R.; Marc, I. CTAB Turbidimetric Method for Assaying Hyaluronic Acid in Complex Environments and under Cross-Linked Form. *Carbohydr. Polym.* **2014**, *112*, 102–108. https://doi.org/10.1016/j.carbpol.2014.05.039.

(26) Willner, I.; Eichen, Y.; Frank, A. J.; Fox, M. A. Photoinduced Electron-Transfer Processes Using Organized Redox-Functionalized Bipyridinium-Polyethylenimine-TiO2 Colloids and Particulate Assemblies. *J. Phys. Chem.* **1993**, *97* (28), 7264–7271. https://doi.org/10.1021/j100130a024.

(27) Kasprzak, A.; Popławska, M.; Bystrzejewski, M.; Łabędź, O.; Grudziński, I. P. Conjugation of Polyethylenimine and Its Derivatives to Carbon-Encapsulated Iron Nanoparticles. *RSC Adv.* **2015**, *5* (104), 85556–85567. https://doi.org/10.1039/c5ra17912b.

(28) Navarrete, J. T. L.; Hernández, V.; Ramírez, F. J. Vibrational Study of Aspartic Acid and Glutamic Acid Dipeptides. *J. Mol. Struct.* **1995**, *348*, 249–252. https://doi.org/10.1016/0022-2860(95)08635-9.

(29) Xu, X.; Jha, A. K.; Harrington, D. A.; Farach-Carson, M. C.; Jia, X. Hyaluronic Acid-Based Hydrogels: From a Natural Polysaccharide to Complex Networks. *Soft Matter* **2012**, *8* (12), 3280–3294.

https://doi.org/10.1039/c2sm06463d.

(30) Liao, Y. H.; Jones, S. A.; Forbes, B.; Martin, G. P.; Brown, M. B. Hyaluronan: Pharmaceutical Characterization and Drug Delivery. *Drug Deliv. J. Deliv. Target. Ther. Agents* **2005**, *12* (6), 327–342. https://doi.org/10.1080/10717540590952555.

(31) Yang, J.; Shi, F. K.; Gong, C.; Xie, X. M. Dual Cross-Linked Networks Hydrogels with Unique Swelling Behavior and High Mechanical Strength: Based on Silica Nanoparticle and Hydrophobic Association. *J. Colloid Interface Sci.* **2012**, *381* (1), 107–115. https://doi.org/10.1016/j.jcis.2012.05.046.

(32) He, M.; Shi, L.; Wang, G.; Cheng, Z.; Han, L.; Zhang, X.; Wang, C.; Wang, J.; Zhou, P.; Wang, G. Biocompatible and Biodegradable Chitosan/Sodium Polyacrylate Polyelectrolyte Complex Hydrogels with Smart Responsiveness. *Int. J. Biol. Macromol.* **2020**, *155*, 1245–1251. https://doi.org/10.1016/j.ijbiomac.2019.11.092.

(33) Chen, Y.; Yan, X.; Zhao, J.; Feng, H.; Li, P.; Tong, Z.; Yang, Z.; Li, S.; Yang, J.; Jin, S. Preparation of the Chitosan/Poly(Glutamic Acid)/Alginate Polyelectrolyte Complexing Hydrogel and Study on Its Drug Releasing Property. *Carbohydr. Polym.* **2018**, *191* (February), 8–16. https://doi.org/10.1016/j.carbpol.2018.02.065.

(34) Treenate, P.; Monvisade, P. In Vitro Drug Release Profiles of PH-Sensitive Hydroxyethylacryl Chitosan/Sodium Alginate Hydrogels Using Paracetamol as a Soluble Model Drug. *Int. J. Biol. Macromol.* **2017**, *99*, 71–78. https://doi.org/10.1016/j.ijbiomac.2017.02.061.

(35) Sadtler, K.; Wolf, M. T.; Ganguly, S.; Moad, C. A.; Chung, L.; Majumdar, S.; Housseau, F.; Pardoll, D. M.; Elisseeff, J. H. Divergent Immune Responses to Synthetic and Biological Scaffolds. *Biomaterials* **2019**, *192* (October 2018), 405–415. https://doi.org/10.1016/j.biomaterials.2018.11.002.

(36) Axpe, E.; Orive, G.; Franze, K.; Appel, E. A. Towards Brain-Tissue-like Biomaterials. *Nat. Commun.* **2020**, *11* (1), 10–13. https://doi.org/10.1038/s41467-020-17245-x.

(37) Yang, J.; Zhao, J. J.; Han, C. R.; Duan, J. F. Keys to Enhancing Mechanical Properties of Silica Nanoparticle Composites Hydrogels: The Role of Network Structure and Interfacial Interactions. *Compos. Sci. Technol.* **2014**, *95*, 1–7.

https://doi.org/10.1016/j.compscitech.2014.02.003.

(38) Zhu, F.; Lin, X. Y.; Wu, Z. L.; Cheng, L.; Yin, J.; Song, Y.; Qian, J.; Zheng, Q. Processing Tough Supramolecular Hydrogels with Tunable Strength of Polyion Complex. *Polymer (Guildf).* **2016**, *95*, 9–17. https://doi.org/10.1016/j.polymer.2016.04.043.

(39) Atalar, B.; Choi, C. Y. H.; Harsh, G. R.; Chang, S. D.; Gibbs, I. C.; Adler, J. R.; Soltys, S. G. Cavity Volume Dynamics after Resection of Brain Metastases and Timing of Postresection Cavity Stereotactic Radiosurgery. *Neurosurgery* **2013**, *72* (2), 180–185. https://doi.org/10.1227/NEU.0b013e31827b99f3.

(40) Jarvis, L. A.; Simmons, N. E.; Bellerive, M.; Erkmen, K.; Eskey, C. J.; Gladstone, D. J.; Hug, E. B.; Roberts, D. W.; Hartford, A. C. Tumor Bed Dynamics after Surgical Resection of Brain Metastases: Implications for Postoperative Radiosurgery. *Int. J. Radiat. Oncol. Biol. Phys.* **2012**, *84* (4), 943–948. https://doi.org/10.1016/j.ijrobp.2012.01.067.

(41) Arno, M. C.; Inam, M.; Weems, A. C.; Li, Z.; Binch, A. L. A.; Platt, C. I.; Richardson, S. M.; Hoyland, J. A.; Dove, A. P.; O'Reilly, R. K. Exploiting the Role of Nanoparticle Shape in Enhancing Hydrogel Adhesive and Mechanical Properties. *Nat. Commun.* **2020**, *11* (1). https://doi.org/10.1038/s41467-020-15206-y.

(42) Zhang, X.; Liu, Y.; Wen, J.; Zhao, Z.; Chen, H.; Liu, X.; Liu, S. Host-Guest Interaction-Mediated Fabrication of a Hybrid Microsphere-Structured Supramolecular Hydrogel Showing High Mechanical Strength. *Soft Matter* **2020**, *16* (14), 3416–3424. https://doi.org/10.1039/d0sm00271b.

(43) Chang, C. W.; Ho, H. O.; Lo, Y. J.; Lee, S. Y.; Yang, Y. R.; Sheu, M. T. Development of Swellable Local Implants of a Polyethyleneimine-Poly(Vinyl Pyrrolidone) (PEI-PVP) Hydrogel as a Socket Filler. *J. Biomater. Sci. Polym. Ed.* **2012**, *23* (17), 2171–2184. https://doi.org/10.1163/092050611X611684.

(44) Satapathy, M. K.; Nyambat, B.; Chiang, C. W.; Chen, C. H.; Wong, P. C.; Ho, P. H.; Jheng, P. R.; Burnouf, T.; Tseng, C. L.; Chuang, E. Y. A Gelatin Hydrogel-Containing Nano-Organic PEI–Ppy with a Photothermal Responsive Effect for Tissue Engineering Applications. *Molecules* **2018**, *23* (6). https://doi.org/10.3390/molecules23061256.

(45) Abraham, B. L.; Toriki, E. S.; Tucker, N. J.; Nilsson, B. L. Electrostatic Interactions Regulate the Release of Small Molecules from Supramolecular

Hydrogels. *J. Mater. Chem. B* **2020**, *8* (30), 6366–6377. https://doi.org/10.1039/D0TB01157F.

(46) Koźmiński, P.; Halik, P. K.; Chesori, R.; Gniazdowska, E. Overview of Dual-Acting Drug Methotrexate in Different Neurological Diseases, Autoimmune Pathologies and Cancers. *Int. J. Mol. Sci.* **2020**, *21* (10). https://doi.org/10.3390/ijms21103483.

(47) Abolmaali, S. S.; Tamaddon, A. M.; Dinarvand, R. A Review of Therapeutic Challenges and Achievements of Methotrexate Delivery Systems for Treatment of Cancer and Rheumatoid Arthritis. *Cancer Chemother. Pharmacol.* **2013**, *71* (5), 1115–1130. https://doi.org/10.1007/s00280-012-2062-0.

(48) Korsmeyer, R. W.; Gurny, R.; Doelker, E.; Buri, P.; Peppas, N. A. Mechanisms of Solute Release from Porous Hydrophilic Polymers. *Int. J. Pharm.* **1983**, *15* (1), 25–35. https://doi.org/10.1016/0378-5173(83)90064-9.

(49) Li, Y.; Lin, J.; Ma, J.; Song, L.; Lin, H.; Tang, B.; Chen, D.; Su, G.; Ye, S.; Zhu, X.; Luo, F.; Hou, Z. Methotrexate-Camptothecin Prodrug Nanoassemblies as a Versatile Nanoplatform for Biomodal Imaging-Guided Self-Active Targeted and Synergistic Chemotherapy. *ACS Appl. Mater. Interfaces* **2017**, *9* (40), 34650–34665. https://doi.org/10.1021/acsami.7b10027.

(50) Jia, Y.; Chen, J.; Liu, W.; Yin, D. Construction of Highly Stretchable Silica/Polyacrylamide Nanocomposite Hydrogels through Hydrogen Bond Strategy. *J. Polym. Res.* **2019**, *26* (5), 1–9. https://doi.org/10.1007/s10965-019-1761-1.

(51) Xia, S.; Song, S.; Ren, X.; Gao, G. Highly Tough, Anti-Fatigue and Rapidly Self-Recoverable Hydrogels Reinforced with Core-Shell Inorganic-Organic Hybrid Latex Particles. *Soft Matter* **2017**, *13* (36), 6059–6066. https://doi.org/10.1039/c7sm01253e.

Supporting Information

Mechanically Tuneable Physical Nanocomposite Hydrogels from Polyelectrolyte Complex Templated Silica Nanoparticles for Anionic Therapeutic Delivery

George Newham[1], Stephen D. Evans[1], Zhan Yuin Ong*[1,2]

1 School of Physics and Astronomy, University of Leeds, Leeds, LS2 9JT, UK.

2 Leeds Institute of Medical Research at St. James's, School of Medicine, University of Leeds, Leeds, LS2 9JT, UK.

*Correspondence to: Z.Y. Ong (z.y.ong@leeds.ac.uk)

Preparation of PEI/Glu Polyelectrolyte Templates

To study the alcohol-induced formation of PEI/Glu PECs, 62.5 µL of 1.28×10^1 mM PEI and 200 µL of 5.44×10^1 mM Glu were added to 737.5 µL of ultrapure water (1 mL total volume). Under stirring, 1.0 – 9.0 mL of IPA was added and then topped up to 10.0 mL total volume with ultrapure water. The final mixture was left to stir at room temperature for 1 h. To form PECs with varied PEI and Glu concentrations, the aqueous reagent volume was maintained at 2.0 mL and 8.0 mL of IPA was added under stirring.

Synthesis of SiNPs without PEI Surface Functionalisation

To synthesise SiNPs without PEI surface functionalisation, an overgrown- arginine (Arg)/polyacrylic acid (PAA) templated synthesis was used based on our previous work[24]. Under magnetic stirring at room temperature, 8.025 mL of ultrapure water, 500 µL of 1.1×10^1 mM PAA, and 1475 µL of 8.6×10^2 mM Arg were added to a round bottom flask. After dispersion in an ultrasonic bath for 5 minutes, 40 mL of IPA was added and the solution was allowed to stir for 1 h. Next, 1 mL of TEOS was added and the mixture was stirred at room temperature for 24 h. The SiNPs were collected and purified by centrifugation and rinsing thrice with ultra-pure water (17,000 × g for 1 h).

***In vitro* Cytotoxicity Testing**

RAW264.7 mouse macrophage and HCT116 human colorectal carcinoma cells were maintained in DMEM growth media that were supplemented with 10% FBS and cultured at 37 °C under an atmosphere of 5% CO_2 and 95% humidified air.

RAW264.7 and HCT116 cells were seeded onto 24-well plates at a density of 1.5×10^5 cells per well. After an overnight incubation, the cells were treated with the nanocomposite hydrogels prepared at 1.2/4.8, 2.4/4.8, and 3.6/4.8 PEI/HA monomer ratios which corresponds to 0.028, 0.056, and 0.084 μM PEI and 0.015 mM HA in 0.5 mL of fresh media for 24 h at 37 °C. Subsequently, the treatment media in each well were replaced with 0.3 mL of growth media and 30 μL of WST-1. The cells were incubated for 2 h at 37 °C before measurement of absorbance at 440 nm using a microplate spectrophotometer (Molecular Devices). Relative cell viability was expressed as $[(A_{sample} - A_{blank})/(A_{untreated} - A_{blank})] \times 100\%$.

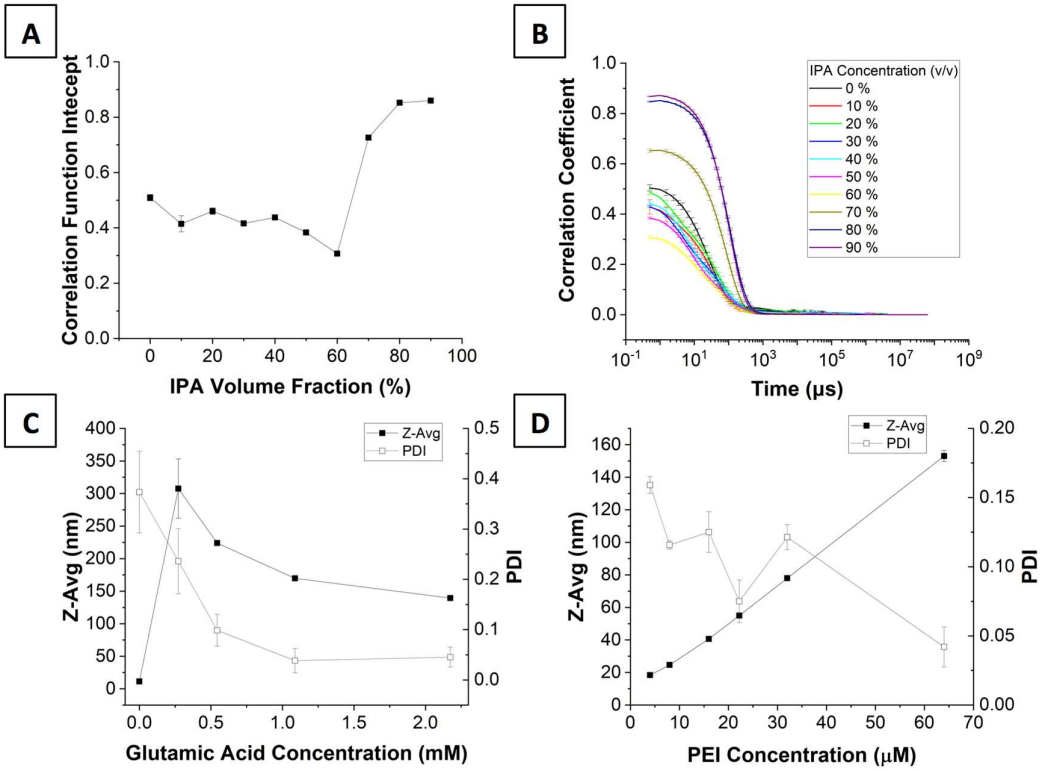

Figure S1. The formation of stable glutamic acid/PEI polyelectrolyte complexes in water/isopropanol (IPA) binary solvents. (A) The effect of IPA volume fraction on the correlation function y-intercept from dynamic light scattering measurements, and (B) the corresponding correlation function curves. Hydrodynamic diameters and PDI values for PECs formed at 80 % IPA with (C) PEI fixed at 64 µM and varying glutamic acid concentrations and (D) glutamic acid fixed at 2.2 mM and varying PEI concentrations.

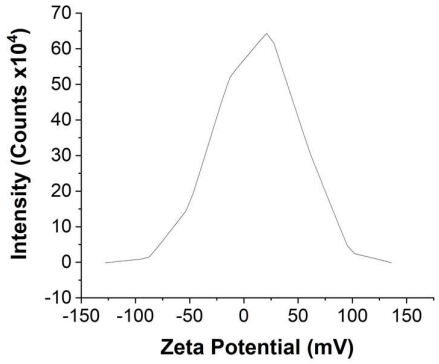

Figure S2. Zeta potential measurements of PEI/Glu PECs prepared in 80 % IPA (v/v) with 1.09 mM of Glu and 64 µM of PEI with a positive surface potential of 38.7 ± 1.5 mV.

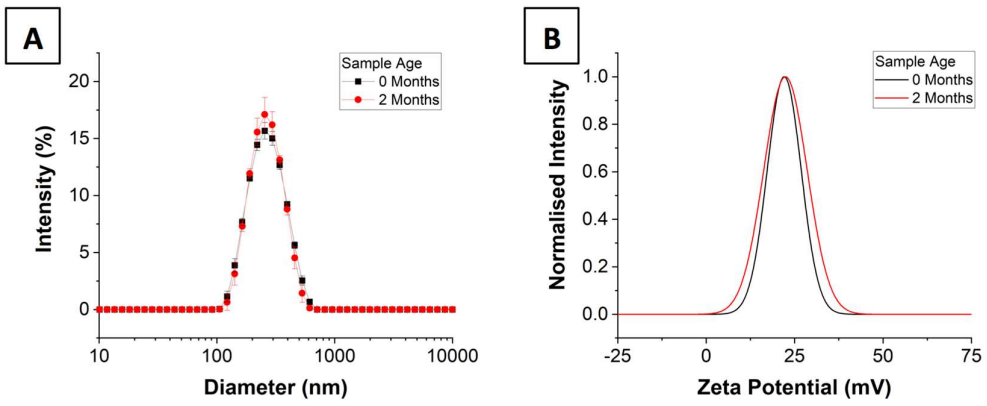

Figure S3. A comparison between freshly prepared PEI-SiNPs and those after 2 months of aqueous storage at room temperature showing (A) DLS hydrodynamic

diameters of 248 ± 3.7 and 247 ± 3.4 nm with PDI values of 0.12 ± 0.01 and 0.09 ± 0.02, and (B) zeta potentials of 22.1 ± 1.1 and 24.2 ± 1.7 mV.

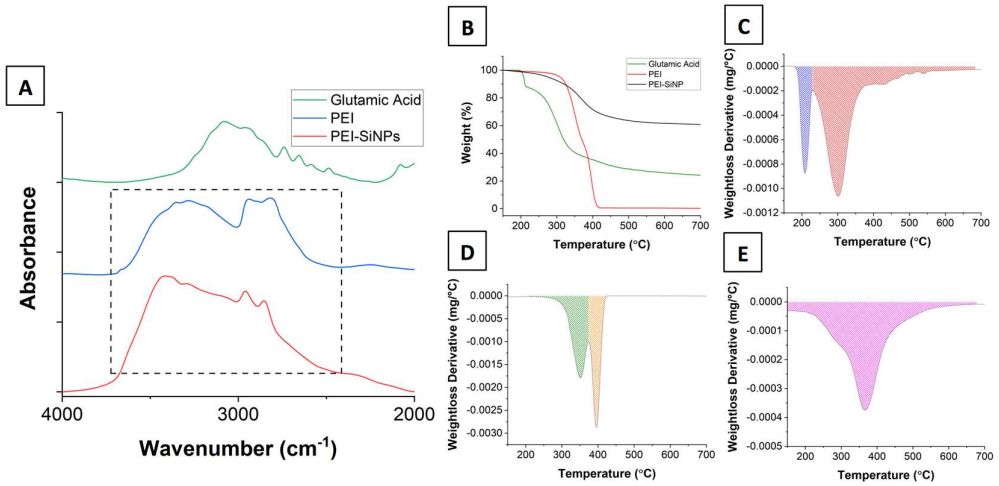

Figure S4. (A) Stacked FTIR spectra of glutamic acid, PEI, and PEI-SiNPs with a dashed box to indicate the region with coexisting peaks between PEI and PEI-SiNPs. (B) Weight loss curves from TGA analysis for glutamic acid, PEI, and PEI-SiNPs, and (C-E) their corresponding 1st derivative curves.

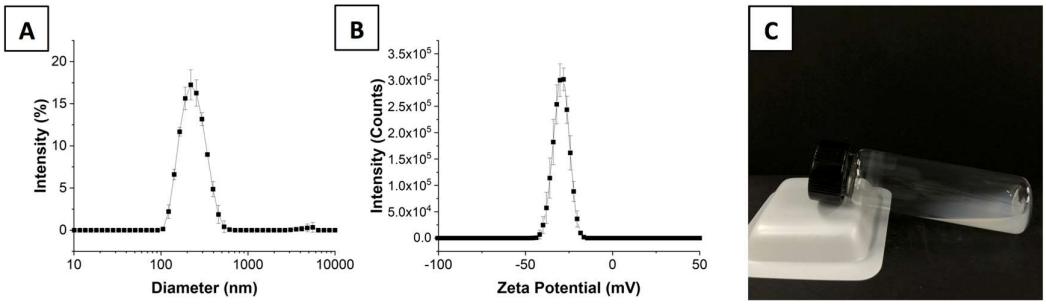

Figure S5. (A) The intensity weighted size distribution for non-PEI functionalised SiNPs measured by DLS with a diameter of 229.8 ± 3.9 nm and PDI of 0.17 ± 0.01. (B) The zeta potential distribution of the SiNPs measured in pH 7.4 PBS with a negative surface charge of -29.5 ± 0.7 mV. (C) A photograph of a mixture of non-PEI

functionalised SiNPs and HA showing no coacervation or gelation even after pH adjustment to ~6.

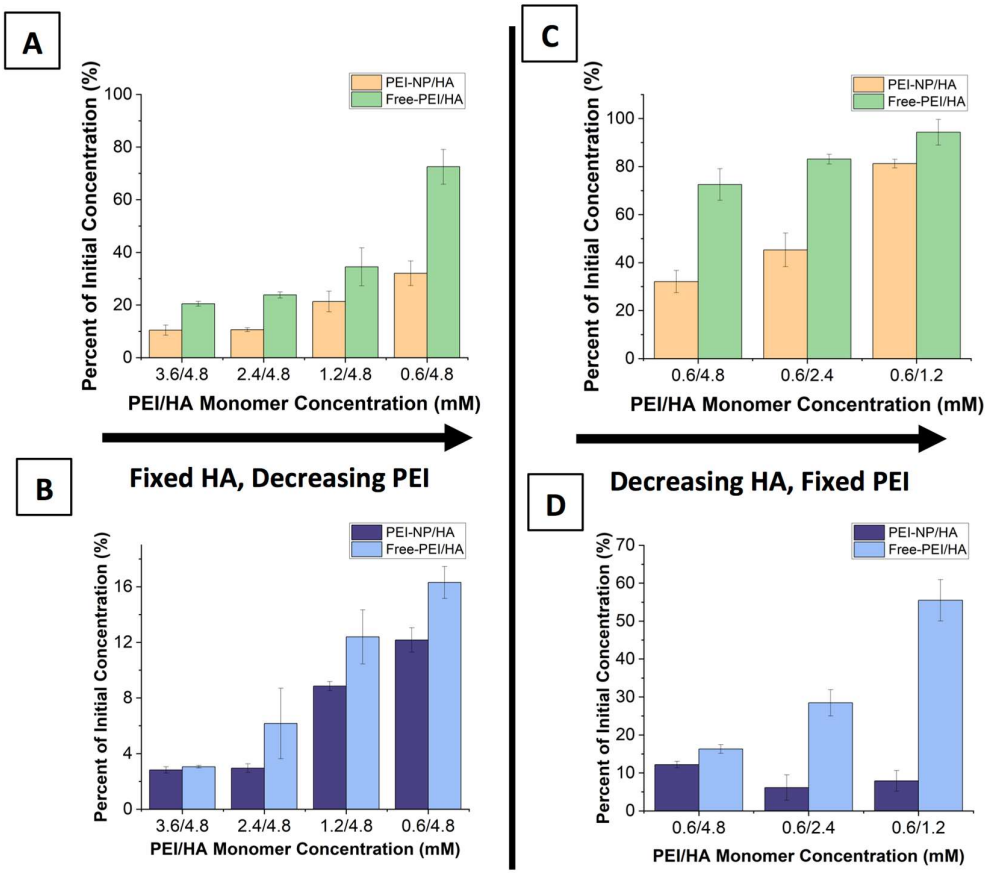

Figure S6. Quantification of the PEI and HA concentration in the supernatant after gel formation normalised to the initial reagent concentration. (A,C) The PEI supernatant concentration as a function of decreasing PEI concentration and decreasing HA concentration, respectively. (B,D) The HA supernatant concentration as a function of decreasing PEI concentration and decreasing HA concentration, respectively.

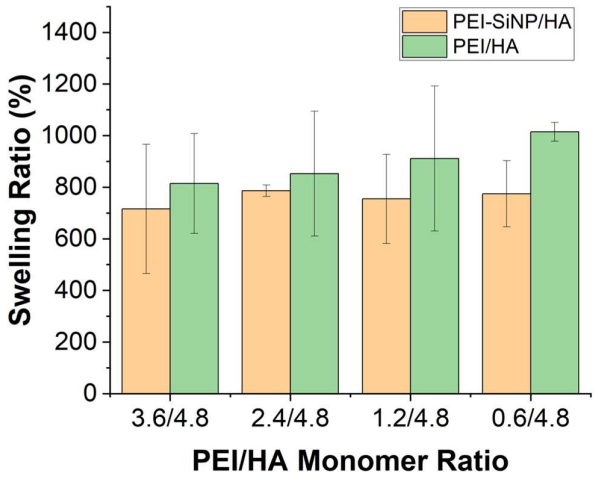

Figure S7. Equilibrium swelling ratios determined in ultrapure water for PEI-SiNP/HA and PEI/HA hydrogels. Values represent mean ± standard deviation from two independent experiments performed in triplicate.

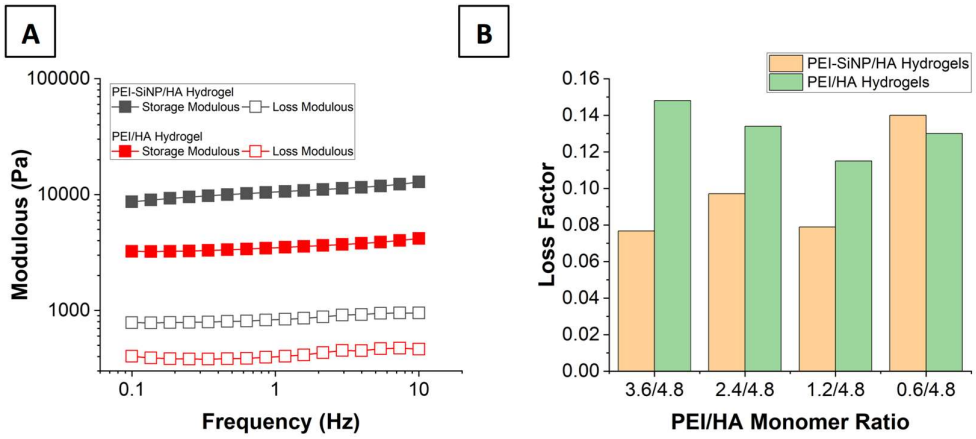

Figure S8. (A) A frequency sweep at 1 % shear strain showing the storage and loss moduli for PEI-SiNP/HA and PEI/HA hydrogels synthesised with PEI/HA monomer ratios of 1.2/4.8. (B) The loss factor at 1 % shear strain and 1 Hz for PEI-SiNP/HA and PEI/HA hydrogels prepared with varied composition.

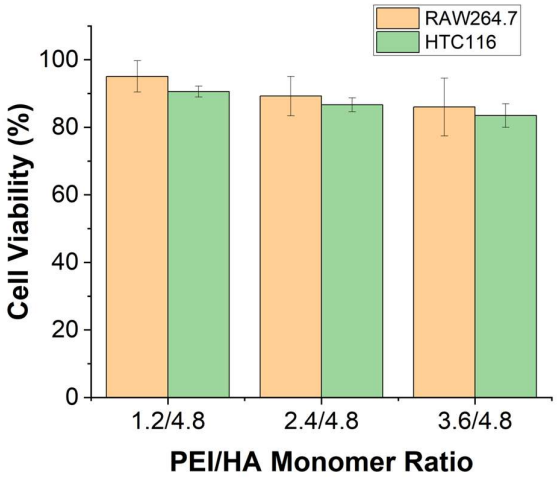

Figure S9. *In vitro* cell viability data determined by WST-1 Assay for PEI-SiNP/HA hydrogels prepared with varied PEI/HA monomer ratios after 24 h incubation with RAW264.7 and HTC116 cells.